G Model
AGMET-4322; No. of Pages 21
ARTICLE IN PRESS
Agricultural and Forest Meteorology xxx (2010) xxx–xxx
Contents lists available at ScienceDirect
Agricultural and Forest Meteorology
journal homepage: www.elsevier.com/locate/agrformet

Vertical structure of evapotranspiration at a forest site (a case study)

Katharina Staudt[a,*], Andrei Serafimovich[a], Lukas Siebicke[a], R. David Pyles[b], Eva Falge[c]

[a] University of Bayreuth, Department of Micrometeorology, 95440 Bayreuth, Germany
[b] University of California, Department of Land, Air and Water Resources, One Shields Avenue, Davis, CA 95616-8627, USA
[c] Max Planck Institute for Chemistry, Biogeochemistry Department, Joh.-J.-Becherweg 27, 55128 Mainz, Germany

ARTICLE INFO

Article history:
Received 1 April 2010
Received in revised form 14 August 2010
Accepted 23 October 2010

Keywords:
Evapotranspiration
Eddy-covariance
Sap flux
Model
In-canopy profiles
Picea abies L.

ABSTRACT

The components of ecosystem evapotranspiration of a Norway spruce forest (*Picea abies* L.) as well as the vertical structure of canopy evapotranspiration were analyzed with a combination of measurements and models for a case study of 5 days in September 2007. Eddy-covariance and sap flux measurements were performed at several heights within the canopy at the FLUXNET site Waldstein–Weidenbrunnen (DE-Bay) in the Fichtelgebirge mountains in Germany. Within and above canopy fluxes were simulated with two stand-scale models, the 1D multilayer model ACASA that includes a third-order turbulence closure and the 3D model STANDFLUX. The soil and understory evapotranspiration captured with the eddy-covariance system in the trunk space constituted 10% of ecosystem evapotranspiration measured with the eddy-covariance system above the canopy. A comparison of transpiration measured with the sap flux technique and inferred from below and above canopy eddy-covariance systems revealed higher estimates from eddy-covariance measurements than for sap flux measurements. The relative influences of possible sources of this mismatch, such as the assumption of negligible contribution of evaporation from intercepted water, and differences between the eddy-covariance flux footprint and the area used for scaling sap flux measurements, were discussed. Ecosystem evapotranspiration as well as canopy transpiration simulated with the two models captured the dynamics of the measurements well, but slightly underestimated eddy-covariance values. Profile measurements and models also gave us the chance to assess in-canopy profiles of canopy evapotranspiration and the contributions of in-canopy layers. For daytime and a coupled or partly coupled canopy, mean simulated profiles of both models agreed well with eddy-covariance measurements, with a similar performance of the ACASA and the STANDFLUX model. Both models underestimated profiles for nighttime and decoupled conditions. During daytime, the upper half of the canopy contributed approximately 80% to canopy evapotranspiration, whereas during nighttime the contribution shifted to lower parts of the canopy.
© 2010 Elsevier B.V. All rights reserved.

1. Introduction

Evapotranspiration is one of the most important components of the water budget in Central European forests. For spruce forests, evapotranspiration can constitute up to 60% of precipitation (Frühauf et al., 1999; Rebmann, 2004). The amount of evapotranspiration of a forest is influenced by physiological and morphological properties of the forest canopy (Baldocchi and Vogel, 1996), and soil properties and soil cover that govern the water vapor exchange at the soil–atmosphere interface (Baldocchi et al., 2000). Further influences are meteorological conditions within and above the canopy such as wind speed, air temperature and humidity. Thus, to understand evapotranspiration of a forest ecosystem, measurements of total ecosystem evapotranspiration by, for example eddy-covariance measurements are not sufficient, as all processes determining evapotranspiration need to be studied. Measurements of forest canopy evapotranspiration profiles with the sap flux and eddy-covariance techniques not only make the partitioning of ecosystem evapotranspiration into its components possible but also assist in understanding the vertical canopy moisture dynamics and its dependence on the vertical structure of plant morphology and in-canopy micrometeorology. A data base comprising measurements of all evapotranspiration components is also needed to validate process-based models to ensure adequate process representations and thus a proper simulation of the various components of evapotranspiration to avoid a compensation of errors in modeling these components in the total ecosystem evapotranspiration (Falge et al., 2005).

Ecosystem evapotranspiration (E_{eco}) consists of four components (here, a similar notation than in Barbour et al., 2005, was

* Corresponding author. Tel.: +49 921 552176; fax: +49 921 552366.
E-mail addresses: katharina.staudt@uni-bayreuth.de (K. Staudt), andrei.serafimovich@uni-bayreuth.de (A. Serafimovich), lukas.siebicke@uni-bayreuth.de (L. Siebicke), rdpyles@ucdavis.edu (R.D. Pyles), e.falge@mpic.de (E. Falge).

0168-1923/$ – see front matter © 2010 Elsevier B.V. All rights reserved.
doi:10.1016/j.agrformet.2010.10.009

Please cite this article in press as: Staudt, K., et al., Vertical structure of evapotranspiration at a forest site (a case study). Agric. Forest Meteorol. (2010), doi:10.1016/j.agrformet.2010.10.009

adopted):

$$E_{eco} = E_c + E_s + E_g + E_w \quad (1)$$

with transpiration from the canopy (E_c), transpiration from the understory vegetation (E_s), evaporation from the ground (E_g) (soil and standing water on understory vegetation), and evaporation from wet canopy surfaces such as from intercepted water (E_w).

The exchange of water vapor of an ecosystem with the atmosphere, thus E_{eco}, is commonly measured with eddy-covariance systems, e.g. at more than 400 sites of various terrestrial ecosystems joined within the FLUXNET network (FLUXNET, 2010).

To monitor the components of E_{eco}, different measurement techniques are available. These components are monitored less often and especially long-term continuous measurements are rare. Apart from assessing one or more components of E_{eco}, Wilson and Meyers (2001) stress differences and limitations of these measurement techniques. Temporal and spatial scale may vary considerably between these methods, making up- or downscaling of the results necessary. Furthermore, underlying assumptions, technical challenges and measurement errors are unique for every measurement system.

The sum of evaporation from the forest floor and transpiration from understory vegetation ($E_g + E_s$) can be estimated using chamber measurements (Rochette and Hutchinson, 2005), the soil water budget (Wilson and Meyers, 2001) or eddy-covariance measurements in the trunk space (Baldocchi and Vogel, 1996; Saugier et al., 1997; Wilson et al., 2000; Roupsard et al., 2006; Jarosz et al., 2008). As the validity of the assumptions of the eddy-covariance method may be questioned in the trunk space of a forest, these measurements have certain limitations. To check the reliability of these data, energy balance closure and spectral analysis are frequently analyzed (Baldocchi and Meyers, 1991; Wilson et al., 2000; Roupsard et al., 2006). Furthermore, the spatial representativeness of measurements within the trunk space is much smaller than of those above the canopy (Baldocchi, 1997). Other errors of eddy-covariance data have been discussed in detail by e.g. Baldocchi (2003).

Sap flux measurements are the most common method to monitor transpiration from the canopy (E_c). Sap flux techniques based on thermometric methods can be divided into three categories: heat pulse velocity methods, heat dissipation methods as well as methods monitoring heat carried away from a controlled heat source by the sap (Burgess et al., 2001). Scaling is required to determine E_c of the stand from sap flux measurements at single trees. Possible relationships found in the literature include the following factors: stem circumference or diameter at breast height, crown projected area, leaf area, basal area, sapwood area, etc. (see review by Wullschleger et al., 1998). The scaling procedure is not straightforward and may include two types of errors (Hatton and Wu, 1995; Granier et al., 2000; Wullschleger and King, 2000; Poyatos et al., 2007): the first is associated with the determination of the average sap flux density, which is very much dependent on the representation of the among tree variability. Secondly, the scaling factors incorporate their very own uncertainties.

In most cases, evaporation from wet surfaces (E_w) is not measured directly. Instead, throughfall and stem flow measurements as well as precipitation measurements above the canopy are performed to assess the amount of rainfall intercepted by the canopy from the difference of precipitation and throughfall/stem flow. Measurements can either be performed at a high temporal resolution using tipping bucket raingauges or collected over a larger time period (Davi et al., 2005; Zimmermann et al., 1999). Recently, a method to estimate rainfall interception directly from a long time series of eddy-covariance measurements was suggested by Czikowsky and Fitzjarrald (2009) and its utility shown for an Amazonian rain forest.

The contribution of the components to E_{eco} varies considerably for different forest ecosystems and different times of the year. For example, above canopy and forest floor eddy-covariance measurements revealed a contribution of $E_g + E_s$ to E_{eco} of less than 10% at a temperate deciduous forest during the growing season (Wilson et al., 2000; Baldocchi and Vogel, 1996), whereas larger contributions were found for the forest floor of a boreal pine forest (50% during a summer period, Baldocchi and Vogel, 1996) and a maritime pine forest (annual contribution of 38%, Jarosz et al., 2008). Accordingly, the contribution of E_c to E_{eco} can be very different for various forest types and seasons at one site: E_c accounted for 65% of E_{eco} at a hardwood-dominated old growth stand (Tang et al., 2006) and a similar contribution was found for a coconut plantation with E_c being 68% of E_{eco} (Roupsard et al., 2006). At a mixed conifer-broad-leaved forest, the contribution of E_c was very different between dry (51%) and wet days (22%) (Barbour et al., 2005), whereas E_c accounted for more than 70% of E_{eco} during winter and spring but only about 50% during summer and fall at a ponderosa pine plantation (Kurpius et al., 2003).

A large fraction of precipitation can be lost due to evaporation of intercepted water with annual losses of 10–60% of precipitation for forests (McNaughton and Jarvis, 1983; Chang, 2006). Factors such as species, stand characteristics and storm conditions have an influence on the magnitude of canopy interception. For example, for two spruce stands at different altitudes in the Eastern Erzgebirge (Eastern Ore Mountains), Germany, 51% of precipitation was lost due to evaporation of intercepted water at the lower elevation site and 28% at the higher site (Zimmermann et al., 1999), due to a larger leaf area index (*LAI*) at the low elevation site and fog deposition at the higher site. Thus, evaporation of intercepted water is an important fraction of the annual evapotranspiration budget of these spruce forests (33% and 44%). McNaughton and Jarvis (1983) report a contribution of 35–75% of interception to the total annual evapotranspiration for different forests.

A large number of soil–vegetation–atmosphere models (SVAT-models), varying in scope, complexity and scale, are available to simulate the exchange of energy and matter of an ecosystem with the overlying atmosphere. Frequently, ecosystem evapotranspiration was compared to eddy-covariance measurements above the canopy. For example, a study by Falge et al. (2005) tested the ability of five models to reproduce the latent and sensible heat fluxes of three sites. These models include modules representing evapotranspiration processes to a different extent. A reasonable agreement was found between all models, but the authors stressed the need for an additional validation of the components of the fluxes, e.g. soil evaporation and transpiration, with parallel measurements, as was done by e.g. Wang et al. (2004), Kellomäki and Wang (1999) and Davi et al. (2005). Multilayer models not only allow the simulation of the different components of the fluxes but also their vertical distribution within the canopy. For SVAT models incorporating higher order closure turbulence schemes, water source-sink profiles or the profiles of the respective latent heat fluxes within the canopy were shown by Park and Hattori (2004) and Juang et al. (2008), but only fluxes above the canopy were compared to measurements. To our knowledge, a comparison of modeled profiles of evapotranspiration and its components to measurements is still missing.

The aim of this paper is to study the partitioning of ecosystem evapotranspiration of a forest (1) into its components and (2) into the contribution from the canopy layers with a combination of measurements and models for the FLUXNET site Waldstein–Weidenbrunnen (DE-Bay). This case study covers a 5-day-period in autumn 2007 and makes use of vertical arrays of eddy-covariance and sap flux measurements. Two stand-scale biosphere–atmosphere models are employed: the 1D multilayer model ACASA (Advanced Canopy-Atmosphere-Soil Algorithm;

Table 1
Eddy-covariance systems at the 'turbulence tower'.

Parameter	Unit	Sampling height [m]	Instrument
Wind vector	$m\,s^{-1}$	36	USA-1, Metek GmbH
		23, 13, 2.25	CSAT3, Campbell Scientific, Inc.
		18, 5.5	Solent R2, Gill Instruments Ltd.
CO_2 concentration, water vapor	$mmol\,m^{-3}$	36, 23, 18, 5.5, 2.25	LI-7500, LI-COR Biosciences
Water vapor	$g\,m^{-3}$	13	Krypton Hygrometer KH-20, Campbell Scientific, Inc.

Pyles et al., 2000) and the 3D model STANDFLUX (Falge, 1997; Falge et al., 2000).

2. Material and methods

2.1. The Waldstein–Weidenbrunnen site

Data for this study were collected at the FLUXNET-station Waldstein–Weidenbrunnen (DE-Bay) during the first period of intensive observation of the EGER project (ExchanGE processes in mountainous Regions, IOP-1). The site is located in a low mountain range, the Fichtelgebirge Mountains in North-Eastern Bavaria (50°08′N, 11°52′E) at an altitude of 775 m a.s.l. The Norway spruce forest (*Picea abies* L., Heindl et al., 1995) at this site is approximately 54 years old, and has a mean canopy height (h_c) of 25 m and a tree density of 577 trees/ha. The horizontal variation of the plant area index at the site as well as the plant area index profile were measured in 2007 with two LAI2000 (LI-COR) instruments (Serafimovich et al., 2008b; Siebicke et al., 2010) and revealed a quite variable plant area index (*PAI*) with a mean value of approximately 5.6 and $5\,m^2\,m^{-2}$, respectively, and a concentration of the main leaf mass within $0.5-0.8h_c$. Understory vegetation is heterogeneous consisting of patches of young spruce trees, small shrubs (*Vaccinium myrtillus*), grasses (*Deschampsia flexuosa*) and mosses. The climate of the region is a continental temperate climate (Dc) according to the effective climate classification by Köppen/Trewatha/Rudloff after Hendl (1991). The annual average temperature at the Waldstein–Weidenbrunnen site is 5.3 °C and annual precipitation sums up to 1162.5 mm (1971–2000; Foken, 2003). Soils at the site are Haplic Podzols (FAO) that developed over granite or gneiss bedrock (Gerstberger et al., 2004). The average slope of the terrain is 2.6° (Thomas and Foken, 2007b). For more information about the site see Gerstberger et al. (2004).

2.2. Experimental setup and data

In the framework of the EGER project, two separate intensive observation periods (IOPs) were conducted at the Waldstein–Weidenbrunnen site in fall 2007 and summer 2008, respectively. Here, data from the first intensive observation period (IOP-1), which took place in September and October 2007 (Serafimovich et al., 2008a), were analyzed.

In addition to a 32 m high tower ('main tower', 50°08′31.2″ N, 11°52′00.8″ E), which permanently provides standard meteorological measurements and hosts an eddy-covariance system on top, a slim 35 m high tower and a 36 m high tower were set up at an approximate distance of 70 m to the south-east and the north-west, respectively. Turbulence measurements were performed at several heights at the slim 35 m high tower ('turbulence tower', 50°08′29.9″N, 11°52′03.1″E) and plant physiological measurements were carried out at the 36 m high, more massive tower ('bio tower', 50°08′32.9″N, 11°51′57.9″E).

Throughout this paper, time data are given in central European time (CET).

2.2.1. Eddy-covariance measurements

During the intensive observation periods, high frequency turbulence measurements were performed on two towers at the Waldstein–Weidenbrunnen site. On the 35-m-tall, slim 'turbulence tower' six eddy-covariance systems were installed consisting of sonic anemometers to detect horizontal and vertical wind components as well as the sonic temperature, and fast-response gas analyzers to measure the density of carbon dioxide and water vapor (Table 1). On the 'main tower' another eddy-covariance system was mounted at the top (Solent R2 Gill Instruments Ltd.; LI-7000, LI-COR Biosciences). As shown by Mauder et al. (2007) different types of sonic anemometers and sensor geometry have no significant influence on the collected data.

The processing of the raw flux data (20 Hz) was done with the TK2 software package, developed at the University of Bayreuth (Mauder and Foken, 2004), including several corrections and quality tests. Quality flags combining the steady state test and the integral turbulence characteristic test after Foken et al. (2004) were calculated and used to filter the flux data. Above the canopy, data with quality flags ≤6 were considered. Inside the forest canopy, the flags determined with the integral turbulence characteristic test were ignored, as the integral turbulence characteristics models implemented in the TK2 software only apply above the canopy (Mauder et al., 2006). Thus, turbulence data inside the canopy were filtered using the quality flag of the steady state test only.

Eddy-covariance data was also analyzed to extract coherent structures from the time series by employing a technique based on the wavelet transform (Thomas and Foken, 2005). The contribution of coherent structures to the total flux, the time scales of coherent structures and the number of coherent structures were derived. Additionally, the distribution of coherent structures in the buoyancy exchange within and above the canopy was used to classify the data into different exchange regimes between the air above the canopy, the canopy, and the trunk space of the forest (Thomas and Foken, 2007a).

The following five exchange regimes were proposed:

- Wave motion (Wa): Linear wave motion is dominant in the flow above the canopy and very low scalar fluxes are associated with linear waves. Thus, the scalar transport is assumed to be minimal and layers to be decoupled.
- Decoupled canopy (Dc): The air above the canopy and the canopy/subcanopy are decoupled. Therefore, there is no transport of energy and matter by coherent structures between these layers.
- Decoupled subcanopy (Ds): The energy and matter transport by coherent structures is limited to the air above the canopy and the canopy, but the subcanopy is decoupled.
- Coupled subcanopy by sweeps (Cs): The transport of energy and matter by coherent structures between the atmosphere, the canopy and the subcanopy is dominated by strong sweep motions, whereas the ejection phase only insignificantly contributes to the exchange.
- Fully coupled canopy (*C*): All observation levels are in a fully coupled state. Both ejection and sweep motions govern the exchange

by coherent structures, which contribute significantly to the transport of energy and matter.

In this study, latent heat fluxes measured with the eddy-covariance method at the 'turbulence tower' within and above the canopy were used to determine the components of the ecosystem evapotranspiration budget in the following way: the latent heat flux (*LE*) at the top of the tower (36 m) represents ecosystem evapotranspiration (E_{eco}). Latent heat fluxes at the lowest measurement height within the trunk space of the forest (2.25 m) capture evapotranspiration of the soil and understory ($E_s + E_g$). Furthermore, the difference of the latent heat flux measured within the trunk space and above the canopy equals canopy evapotranspiration $E_c + E_w (E_c + E_w = E_{eco} - (E_s + E_g) = LE(36\,\mathrm{m}) - LE(2.25\,\mathrm{m}))$. Under the assumption of a dry canopy, thus of zero evaporation from intercepted water (E_w), this difference yields canopy transpiration (E_c) directly.

2.2.2. Sap flux measurements

The 'heat ratio method' (HRM) allows the measurement of sap flux in woody parts of tree trunks and branches and the derivation of transpiration estimates for trees and stands (Green and Clothier, 1988; Burgess et al., 1998, 2000; Green et al., 2003). By measuring the amounts of water transferred between different levels within a tree, we sought to generate an independent measure of in-canopy vertical transpiration profiles for the evaluation of the models. We installed sap flux velocity probes (HMR-30, ICT International Pty Ltd., Armidale/Australia) at six different heights above the forest floor (1.4, 11.7, 14.8, 17.2, 20.2 and 22.6 m) in the stems of two *P. abies* L. trees, situated on the south side of the 'bio tower'. Sap flux measurements in the tree trunk (at 1.4 m) allowed the estimation of the total amount of water transpired by the entire tree. From the installation at 22.6 m we derived the amount of water transpired by the needled branches connected to the stem above that height. From the difference in water flow between subsequent installation levels we inferred the amount of water transpired by the branches growing between the two installation heights.

The sensors consist of three needle-shaped probes with thermocouples, which were inserted radially into the xylem. Upstream and downstream temperature probes were placed in −0.005 and +0.005 m from the position of the heated sensor. All sensors were installed on the north side of the stem to reduce effects due to circumferential heterogeneity in sap flow (Nadezhdina et al., 2002; Caylor and Dragoni, 2009; Dragoni et al., 2009). To account for differences in the sap flux velocity at different radial depths, each sensor contained two thermocouple pairs to measure sap flux at 0.0125 and 0.0275 m depth within the xylem. Side-by-side comparison of sensors installed close to each other in the stem revealed random errors of only 12.3% for the outer and 10.9% for the inner thermocouple. Hence, only a single sensor was installed at each height, in order to obtain a finer vertical resolution of the transpiration profiles. Sensitivity of the sensors to air temperature fluctuations was counteracted by covering the installed probes with a layer of bubble-wrap and reflecting aluminum foil. For each sensor installed, the cross-sectional area of sapwood was derived at the end of the measuring period, taking circumference measurements using a tape-measure, and total depth of the sapwood from cores using a wood borer (Suunto, Finland).

Heat pulses were released every 10 min, and thermocouple readings recorded with a datalogger (SL5 Smart Logger, ICT International Pty Ltd, Armidale/Australia). Sap flux velocity readings were corrected for probe misalignment, differences in thermal diffusivity (calculated from measured wood density), and wounding effects, following Burgess et al. (2001). A sudden baseline shift in one of the sensors (disturbance of the sensor setup after a period of high wind speeds) was corrected after normalizing the data using an undisturbed data set as reference. For each thermocouple pair, the data were multiplied by the appropriate cross-sectional area of sapwood, and density of water, resulting in an inner and outer water flux reading (volume per hour, $\mathrm{kg\,h^{-1}}$). The ring-shaped sapwood area represented by the outer thermocouple reading was assigned a radial depth of 0.02 m. The radial depth for the inner thermocouple reading was obtained by subtracting 0.02 m from total sapwood depth.

Stand estimates of canopy transpiration (E_c) were derived from weighted sums of the sap flux of the two trees with sap flux sensor profiles, up-scaled to stand estimates using the number of trees per hectare (577 trees/ha) and hourly correction factors accounting for the fact that the two trees were much larger than the average of the stand. The correction factors were derived as follows: during a second intensive observation period (IOP-2) sap flux sensors were installed at 1.4 m in seven trees representing the range of diameters at breast height observed in the entire stand. From those measurements a stand estimate of canopy transpiration was calculated and used as a reference to scale the stand estimate derived from the profile trees.

Measured values of sap flux were converted from $\mathrm{kg\,h^{-1}}$ to $\mathrm{W\,m^{-2}}$ by multiplication with the latent heat of evaporation ($2.45\,\mathrm{MJ\,kg^{-1}}$ at 20 °C). Stand estimates for each canopy level were derived from summation of inner and outer water flux readings, and the final values for each level were averaged to 30 min values.

To compare the sap flux profiles to the eddy-covariance measurements, cumulative transpiration profiles were calculated from the sap flux signals as follows: at the top of the tree a sap flux of zero was assumed. For all layers, the sap flux signal measured at the top height of the layer was subtracted from the value at the bottom height of the layer. These differences were summed, thus the top height value is the sum of all differences and represents the total transpiration (E_c) of the profile. As the two trees chosen for sap flux profile measurements were larger than the average of the stand, their average tree height of 26.5 m was used to scale measurement height, whereas for eddy-covariance measurements $h_c = 25$ m was utilized.

2.2.3. Supporting meteorological measurements

At the 'main tower' and at a clearing at an approximate distance of 250 m, standard meteorological measurements are performed year round (for details about the measurement devices see Table 2). 'Main tower' measurements comprised in- and above canopy profiles of wind, temperature and humidity, as well as all components of the radiation budget which were measured at the top of the tower above the canopy. During the intensive observation periods, radiation measurements were also performed in the trunk space of the forest at 2 m. At the foot of the tower, soil parameters (volumetric soil moisture, soil temperature) were measured. Precipitation rate and atmospheric pressure were available from a weather station at a clearing nearby.

The models utilized in this study require half-hourly meteorological input values. Above canopy values for air temperature, specific humidity, mean wind speed and down welling short- and long-wave radiation were provided by the 'main tower' standard measuring program, whereas precipitation rate and air pressure were supplied by the measurements at the clearing. Carbon dioxide concentration was provided by the LI-7000 measurement at the top of the 'main tower'. Gaps in the meteorological driving variables were seldom, and were filled with linear interpolation methods. The ACASA model (Pyles et al., 2000) additionally needs initial profiles of soil temperature and soil moisture.

Table 2
Meteorological parameters measured at the 'main tower' and the clearing that are relevant for this study.

Parameter	Unit	Sampling height [m]	Instrument, manufacturer
Routine measurements at the 'main tower'			
Dry bulb temperature	°C	0.05, 2, 5, 13, 21, 31	Vent. psychrometer (Frankenberger, 1951), Theodor Friedrichs & Co
Wet bulb temperature	°C	0.05, 2, 5, 13, 21, 31	Vent. psychrometer (Frankenberger, 1951), Theodor Friedrichs & Co
Mean wind speed	$m\,s^{-1}$	2, 4.6, 10, 16.5, 18, 21, 25, 31	Cup anemometer, Theodor Friedrichs & Co
Wind direction	°	32	Wind vane W200P, Vector Instruments
Short-wave radiation	$W\,m^{-2}$	30	CM14 Pyranometer, Kipp & Zonen
Long-wave radiation	$W\,m^{-2}$	30	CG2 Net pyrgeometer, Kipp & Zonen
Soil moisture	%	−0.1, −0.5	TRIME-EZ TDR sensors, IMKO GmbH
Soil temperature	°C	−0.02, −0.05, −0.1, −0.2, −0.5, −0.7, −1.0, −2.0	Pt-100 thermometers Electrotherm GmbH
Additional measurements at the 'main tower'			
Short-wave radiation	$W\,m^{-2}$	2	CM24 albedometer, Kipp & Zonen
Long-wave radiation	$W\,m^{-2}$	2	Eppley PIR Pyrgeometer, Eppley Laboratory, Inc.
Routine measurements at the clearing			
Precipitation rate	mm	1	OMC 212, Adolf Thies GmbH & Co. KG
Air pressure	hPa	2	Barometric pressure sensor, Ammonit Gesellschaft für Messtechnik mbH

2.3. In-canopy modeling

Two stand-scale biosphere–atmosphere models were employed for the simulation of canopy exchange, the canopy-surface-layer model ACASA (Advanced Canopy-Atmosphere-Soil Algorithm; Pyles, 2000; Pyles et al., 2000) and the microclimate and gas exchange model STANDFLUX (Falge, 1997; Falge et al., 2000). The outstanding feature in the simulation of the exchange of energy and matter within and above the canopy in ACASA is a third-order closure method to calculate the turbulent transfer within and above the canopy (Meyers and Paw, 1986, 1987). Whereas ACASA is a one-dimensional model, the STANDFLUX model explicitly considers the spatial heterogeneity of the stand as it integrates three-dimensional information on stand structure and vertical information on stand microclimate to compute spatial light interception and spatial canopy gas exchange. The ACASA model has been used for several high- and low-vegetation sites, such as an old-growth forest (Pyles et al., 2000) and a maquis site (Marras, 2008) and was recently adapted to the Waldstein–Weidenbrunnen site (Staudt et al., 2010). STANDFLUX has previously been applied to the Waldstein–Weidenbrunnen site, among other sites, by Falge et al. (2000). In the following, basic features of the two models that are especially relevant for the simulation of water exchange are explained.

2.3.1. The ACASA model

In the multilayer model ACASA vegetation is partitioned in 10 equally spaced layers and its structure has to be defined by the user, specifying canopy height, total *LAI* and the *LAI* profile. The model domain extends to twice the canopy height with 10 equally spaced atmospheric layers, and includes 15 soil layers with variable depths.

For the calculation of fluxes, the model distinguishes between different surface types: leaves, large and small stems, and buildings that can either be dry, wet or snow covered. Fractions of these surfaces for each layer are first determined by the fractions of total area index per layer and, secondly, calculated within the interception submodel, as will be explained below. Furthermore, a spherical leaf angle distribution with nine leaf angles is assumed for sunlit leaves. For each layer, the fraction of shaded and sunlit leaves is determined within the short-wave radiation submodel which follows the basic ideas as outlined in Meyers (1985).

Heat and moisture fluxes are calculated with a gradient resistance formulation for all surface types and leaf angles. As this study concentrates on evapotranspiration, only the calculation of the moisture flux divergences is shown here:

$$\frac{d\left\langle w'q'\right\rangle}{dz} = \frac{q_s(T_s) - q_a}{r_s + r_b} \cdot \frac{1}{h_l} \tag{2}$$

with r_s and r_b being the stomatal and aerodynamic resistances, q_a the specific humidity of the air and $q_s(T_s)$ the specific humidity at saturation vapor pressure for surface temperature T_s and h_l the layer height. For an accurate calculation of surface temperatures of leaves, stems and the soil, even for conditions when these may deviate significantly from ambient air temperatures, a fourth-order polynomial following Paw and Gao (1988) is used.

Stomatal resistances of dry leaves (r_s) are computed within the plant physiological submodels where the Ball–Berry stomatal conductance calculations (Leuning, 1990; Collatz et al., 1991) and the Farquhar and von Caemmerer (1982) photosynthesis equations are combined following Su et al. (1996). The calculation of aerodynamic resistances (r_b) for both sensible and latent heat transfer considers a free convection and a forced convection component. For the calculation of soil evapotranspiration, the soil surface resistance, which matches r_s in the calculation of the moisture flux divergence, is calculated as a function of soil moisture and also considers free convection.

The moisture flux divergence for each layer is derived by summing up the calculated moisture flux divergences for all surface types, which are weighted according to their occurrence. A negative moisture flux according to the formula above can occur for negative gradients, which represents dew formation on the leaf surfaces.

The ACASA model includes an interception submodel for the simulation of the amount of precipitation intercepted by the forest canopy. The total capacity of canopy water storage depends on the *PAI* and is distributed between the canopy layers according to their fraction of *PAI*. When precipitation occurs, these storages are successively filled and precipitation reaching lower layers diminishes accordingly. The model also accounts for water already standing on the canopy. The fractional area of wet leaves depends on the fraction of water filled storages and is limited to a maximum of 25% of the leaf surfaces. Evaporation from interception stores is calculated using equation (2), where stomatal resistances r_s for wet and snow covered leaves are set to zero. The amount of water evaporated from the interception stores within a certain timestep is then subtracted from the canopy water storage.

Simulations of soil moisture and soil temperature are performed with a soil module that was adapted from MAPS (Mesoscale Analysis and Prediction System; Smirnova et al., 1997, 2000).

The ACASA model provided all components of ecosystem evapotranspiration as well as in-canopy profiles of E_c and of E_w.

2.3.2. The STANDFLUX model

The STANDFLUX model consists of a leaf or branch gas exchange module, a three-dimensional, single tree light interception and gas exchange module, and the three-dimensional forest stand gas exchange model. It describes canopy water vapor and carbon dioxide exchange based on rates calculated for individual trees and as affected by local gradients in photon flux density (*PFD*), atmospheric humidity, atmospheric carbon dioxide concentration, and air temperature. Direct, diffuse, and reflected *PFD* incident on foliage elements is calculated for a three-dimensional matrix of points superimposed over the canopy. The model was used to calculate forest radiation absorption, net photosynthesis and transpiration of single trees, and gas exchange of the tree canopy. Model parameterization was derived for the Waldstein–Weidenbrunnen site. Parameterization included information on vertical and horizontal leaf area distribution, tree positions and tree sizes, determined in 2007 and 2008.

Gas exchange was modeled using specific sets of physiological parameters for top, middle, and bottom canopy. A portable gas exchange system (GFS3000, Walz, Effeltrich, Germany) was used to monitor the response of needle gas exchange under assorted conditions during the field campaigns. Stomatal conductance depends on a series of micrometeorological factors like incident radiation, leaf temperature, relative (or absolute) humidity, leaf internal CO_2 concentration, but also on leaf nutrition and ontogenetic factors. Branch gas exchange of *P. abies* L. was measured with the GFS3000 in September/October 2007 at the Waldstein–Weidenbrunnen site at three different heights in the forest canopy with the objective of understanding spatial trends in the gas exchange response. Branches analyzed were growing between 10 and 11 m (bottom), 15 and 16 m (middle), and 20 and 21 m (top level) above ground. For example, in IOP-1 the needles exhibited a photosynthesis rate at light saturation at 16 °C (*Pmax*) of 10.6 μmol CO_2 m^{-2} s^{-1} at the top, while only 5.3 and 4.1 μmol m^{-2} s^{-1} were observed at the middle and bottom levels, respectively, representing different physiological behavior in response to shade adaptation. The needles in the top canopy had larger rates of *Pmax* compared to subcanopy leaves. Gas exchange responses to environmental factors were analyzed with a physiologically based model of the Farquhar type. Parameter estimates for describing carboxylase kinetics, electron transport, and stomatal function were derived, utilizing information from both single factor dependencies to light, temperature, CO_2 concentration, and relative humidity, and diurnal time course measurements of gas exchange. Data subsets were used for testing the model at the branch level. Most of the observed variation in gas exchange characteristics was explained with the model: a number of systematic errors were eventually related to light acclimation, nutrition, and needle age. Sets of parameter values for top, middle, and bottom of the canopy have been obtained for application with spruce, for example for use in calculating canopy flux rates. The value of the model for estimating fluxes between the forest and the atmosphere has been evaluated together with measurements at the stand level (Falge and Meixner, 2008).

Soil evaporation was modeled employing the multiple-layered soil water balance model of SVAT-CN (Falge et al., 2005). The soil modules there comprise a hybrid between a layered bucket model and classical basic liquid flow theory (Richard, 1931), numerically solved after Moldrup et al. (1989, 1992), and parameterized after van Genuchten (1980) and Rawls and Brakensiek (1989). Soil heat transport is modeled after Campbell (1985). Transpirational demand is distributed to layers proportional to soil resistance, which itself is a function of hydraulic conductivity and root density.

Interception pool size is modeled as a function of *LAI* profile. Interception pools are filled during precipitation events based on sky view factors, and filling status of interception pools, with a downward cascade of potential overflow of upper canopy pools to interception pools deeper in the canopy. Interception loss is limited by an energy balance approach to wetted leaf area. The subroutines have been compared against other models and tested vigorously using data from the VERTIKO project (Falge et al., 2005), demonstrating the ability to simulate water balance components with reasonable accuracy.

PAI profiles were derived from horizontally averaging a virtual 3D forest stand constructed from forest inventory data measured during 2007 and 2008: [*x*, *y*]-positions and circumference at breast height (*CBH*, m) of the 638 trees within the fenced area of the Waldstein–Weidenbrunnen were measured with a forestry laser (Criterion 400, Laser Technology Inc. (LTI)), and a tape-measure, respectively. For 131 trees crown length (*L*, m) and tree heights (*H*, m) were determined using an inclinometer (Suunto, Finland). From those data we derived allometric relationships between *CBH* and tree height ($H = 11.087 \cdot Ln(CBH) + 22.101$, $R^2 = 0.74$), and *CBH* and crown length ($L = 11.148 \cdot Ln(CBH) + 12.92$, $R^2 = 0.70$), for calculation of *L* and *H* of the remaining 207 trees. The basal area of crown projections (*AC*, m^2) was calculated from *CBH* ($AC = -13.401 \cdot CBH^3 + 42.932 \cdot CBH^2 - 17.062 \cdot CBH + 4.161$, $R^2 = 0.90$), using data of 41 40–70-year-old *P. abies* trees analyzed in the Lehstenbach catchment by Alsheimer (1997). Cylindrical crown shapes were calculated from *AC* and *L*, and positioned in the virtual 3D stand according to the [*x*, *y*]-positions of each tree, providing the volumes for the 3D distribution of leaf area. Initial estimates of total leaf and stem area of each tree and distribution of leaf and stem area within the crown were calculated from relationships with *CBH* as derived by Alsheimer (1997) and Falge et al. (2000). From the virtual 3D stand a virtual horizontal *PAI* distribution was calculated. Using the parameters of the relationship between total leaf area of each tree and *CBH* as fitting parameters, the calculated horizontal *PAI* distribution was fitted to match the measured horizontal *PAI* distribution.

Similarly to the ACASA model, all components of ecosystem evapotranspiration were provided by the STANDFLUX model and its soil and interception modules. Furthermore, in-canopy profiles of E_c and E_w were available.

2.3.3. Model parameterization

The two models require the definition of a range of input parameters by the user (for a list of input parameters of the ACASA model see Staudt et al., 2010). As we intended to compare the two models not only to measurements but also to each other, we tried to use the same parameter sets in the two models. These input parameters were, as far as possible, derived from independent measurements at the site. As explained in Chapter 2.3.2 leaf gas exchange measurements at several heights within the canopy were used to parameterize the Farquhar type model within the STANDFLUX model. These plant physiological parameters obtained for several heights within the canopy were converted to the equations used in ACASA. Furthermore, the forest inventory data measured in 2007 and 2008 served as the data base for the plant morphological parameters, such as the *LAI* and the canopy height of the stand. The virtual 3D stands created from the measurements for the STANDFLUX model (Chapter 2.3.2) was sliced into 29 horizontal layers of 1 m depth for calculating the 1D *PAI* distribution to be used in ACASA (see Fig. 6c). For input parameters that were not measured within the EGER project, values were adopted from the literature on the Waldstein–Weidenbrunnen site or about other spruce forest stands (see Staudt et al., 2010 for a list of references). As both model parameterizations were derived from independent measurements at the site or literature values, and no tuning of the parameters has been performed to match model results with evapotranspiration data, the models represent independent estimates of evapotranspiration for use in model–model and model–data intercomparison.

2.3.4. Comparability of profiles and calculation of error measures

The installation heights of eddy-covariance measurements and sap flux measurements within the profile as well as layer heights in the ACASA and STANDFLUX models were different, yet optimized to fully exploit the explanatory potential of the various approaches. For comparability of measurements and models, profiles were interpolated using an Akima interpolation scheme after Akima (1978) implemented in the R-package 'akima' (R Development Core Team, 2008). The eddy-covariance measurement heights were defined as reference heights for comparison of cumulative profiles, whereas the contributions of the canopy layers were calculated for 10 equally spaced measurement heights (layer height $0.1h_c$).

To evaluate the agreement of model results and measurement values (model-predicted values P) with the reference measurements (observed values O, here either eddy-covariance or sap flux measurements), several error measures were calculated. Willmott (1982) suggests not only assessing model performance using the coefficient of agreement (R^2), but also computing difference measures. Here, the mean bias error (*MBE*), the root mean square error (*RMSE*) the mean absolute error (*MAE*) and the index of agreement (d) are reported (Willmott, 1982):

$$MBE = N^{-1}\sum_{i=1}^{N}(P_i - O_i) \tag{3}$$

$$RMSE = \left[N^{-1}\sum_{i=1}^{N}(P_i - O_i)^2\right]^{0.5} \tag{4}$$

$$MAE = N^{-1}\sum_{i=1}^{N}\left|P_i - O_i\right| \tag{5}$$

$$d = 1 - \left[\frac{\sum_{i=1}^{N}(P_i - O_i)^2}{\sum_{i=1}^{N}\left(\left|P_i'\right| - \left|O_i'\right|\right)^2}\right], 0 \le d \le 1 \tag{6}$$

with the number of cases N and where $P_i' = P_i - \overline{O}$ and $O_i' = O_i - \overline{O}$ and $\overline{O}$ is the mean of the observed variable.

3. Results

3.1. Meteorological conditions

For this analysis, we concentrate on a 5-day-period in September 2007 (20–24 September, DOY 263–267) during which sunny weather conditions prevailed. During these 5 days, no precipitation occurred and high radiative input was received (Fig. 1), however 14.4 mm of rainfall occurred 2 days before this fair weather period. The air and soil cooled down, the vapor pressure deficit became minimal and soil moisture increased. After the rain event of DOY 261, temperatures and vapor pressure deficits (*vpd*) rose and soil moisture depleted again, but it took some days to reach the pre-event values. The comparison of within and above canopy measurements indicated the formation of gradients of vapor pressure deficit and air temperature between the canopy and the air above during the afternoon and night, and these gradients increased towards the end of the fair weather period. Only about 8% of incoming short-wave radiation (R_g) reached the floor of the spruce forest. Wind direction was south–west to west for the first days during the study period and turned to south–east and south in the evening on day 265.

Table 3
Error measures for the comparison of time series for E_c compared to eddy-covariance measurements (Fig. 3b). *MBE*, *MAE* and *RMSE* are expressed as the percentage of the mean canopy top eddy-covariance measurement value (daytime (N = 87): 100 W m^{-2}, nighttime (N = 65): 19 W m^{-2}).

Model/Measurement	*MBE* (%)	*MAE* (%)	*RMSE* (%)	d	R^2
Daytime					
ACASA ($E_c + E_w$)	−9.7	23.7	31.9	0.85	0.67
ACASA (E_c)	−12.8	25.9	34.0	0.84	0.63
STANDFLUX ($E_c + E_w$)	−13.1	23.9	32.4	0.86	0.67
STANDFLUX (E_c)	−16.4	26.7	35.4	0.84	0.63
Sap flux measurements (E_c)	−15.7	29.5	37.6	0.82	0.56
Nighttime					
ACASA ($E_c + E_w$)	−46.7	69.3	83.1	0.38	0.0001
ACASA (E_c)	−50.4	71.6	85.4	0.39	0.0002
STANDFLUX ($E_c + E_w$)	−86.1	90.4	107.3	0.41	0.01
STANDFLUX (E_c)	−86.1	90.4	107.3	0.41	0.01
Sap flux measurements (E_c)	8.2	67.4	88.2	0.47	0.01

Mean daytime and nighttime temperature and *vpd* profiles indicate higher temperatures and *vpd*s during day than at night for all canopy heights (Fig. 2). Whereas temperatures and *vpd*s constantly decreased with decreasing height in the canopy during nighttime, there was a maximum at $0.84h_c$ for temperature and *vpd*, with higher than above canopy values during daytime. Mean daytime and nighttime wind speed profiles had a similar shape within the canopy with a local minimum of wind speed at $0.5h_c$ and a secondary maximum in the trunk space of the forest, which is more pronounced during nighttime (Fig. 2c).

3.2. Evapotranspiration components: time series

Ecosystem evapotranspiration (E_{eco}) and its components for the 5 days fair weather period are displayed in Fig. 3 together with the coupling regimes. Both models underestimated daytime E_{eco} with maximum discrepancies of 55 (104) W m^{-2} for ACASA, and 69 (134) W m^{-2} for STANDFLUX (Fig. 3a). The extreme values (brackets) were associated with a single period on day 266 (11:00–13:00) with winds turning from SSE to NW and back to SSE. In the morning hours, agreement of models and eddy-covariance measurements was better, including time steps of underestimation but also overestimation by the models (especially ACASA). STANDFLUX largely underestimated nighttime E_{eco} (max. deviation 43 W m^{-2}), whereas ACASA estimates were closer to eddy-covariance measurements (max. deviation 25 W m^{-2}).

Canopy evapotranspiration ($E_c + E_w$) measured with the eddy-covariance method was calculated from the difference between the above canopy measurements (36 m) and the measurements in the trunk space (2.25 m). Under dry conditions, which was our initial assumption, this difference is equal to canopy transpiration (E_c) and is displayed as such in this and the following figures. Maximum daytime E_c (Fig. 3b) as measured with the eddy-covariance method was larger than model estimates and sap flux measurements. Agreement of eddy-covariance measurements and modeled fluxes became better towards the end of the 5-day-period; with values in the model results which, although larger, were still too low (see also Fig. 4). Daytime agreement with *MAE* of 23.7% (ACASA) and 23.9% (STANDFLUX) was better than at nighttime (Table 3), when the models considerably underestimated E_c with *MAE* of 69.3% (ACASA) and 90.4% (STANDFLUX). Sap flux measurements displayed daytime maximum values that increased from only the first to the second day but were similar throughout the last 3 days, thus the daytime underestimation compared to eddy-covariance measurements throughout the 5-day-period remained the same, with a daytime *MAE* of 29.5% (Table 3). Sap flux measurements and modeled E_c agreed very well during 3 of the 5 days. On the second day, E_c estimates from sap flux measurements were larger

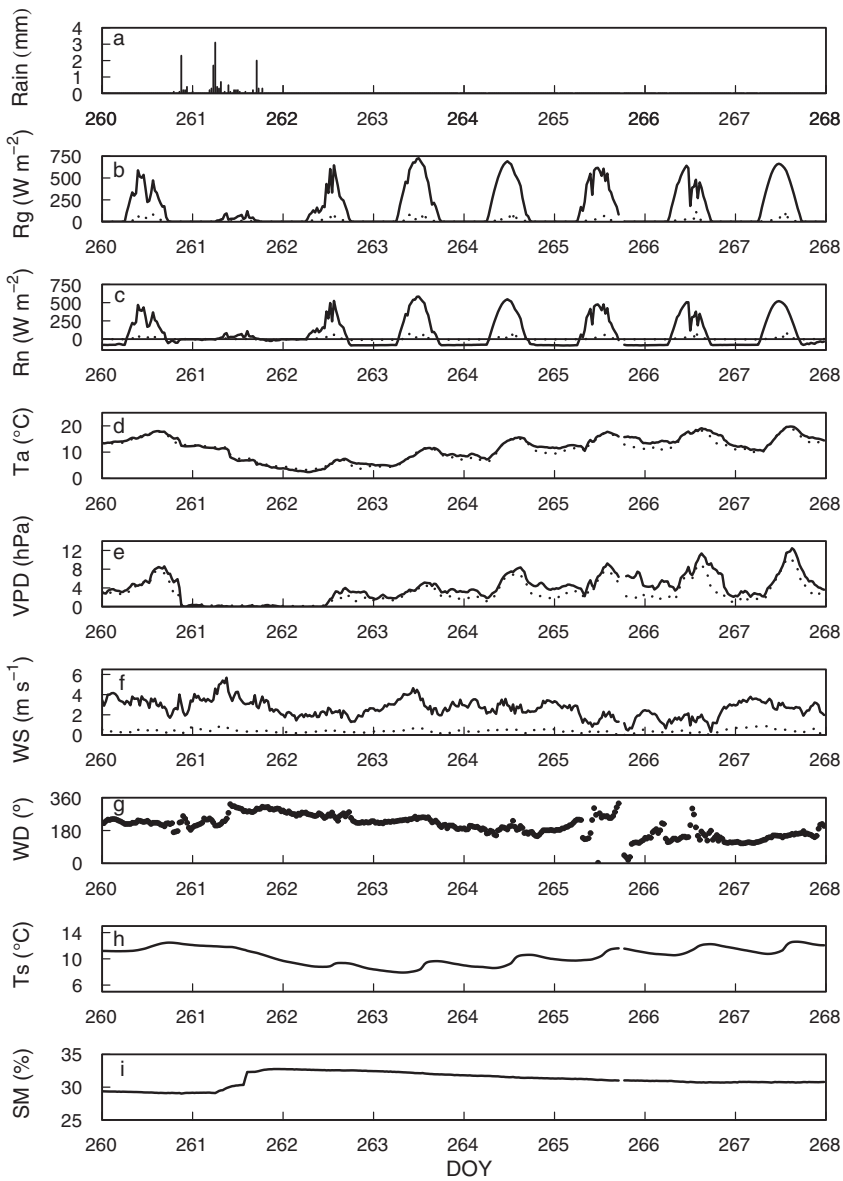

Fig. 1. Meteorological conditions for 17–24 September 2007 (DOY 260–267). Precipitation (a) at the clearing nearby; global radiation (b), net radiation (c), air temperature (d), vapor pressure deficit (e), wind speed (f) and wind direction (g). Solid lines represent data from the top of the 'main tower' (30–32 m, see Table 2), dotted lines data from the trunk space of the forest (2.25 m). Soil temperature (*h*) and soil moisture (*i*) measured at 10 cm depth close to the base of the 'main tower'. The last 5 days are the period (20–24 September, DOY 263–267) on which this study concentrates.

than modeled values but still lower than eddy-covariance estimates, whereas on the last day sap flux estimates were lower than modeled E_c as well as eddy-covariance estimates. Alltogether, daytime *MAE* of the models compared to sapflux measurements were smaller than 20% (Table 3). At least for the first 2 days E_c from sap flux measurements is delayed when compared to the other curves (Fig. 3b). A time shift of 0.5 h compared to transpiration measured with the eddy-covariance systems revealed the best correlation in terms of R^2. From a hydraulic point of view, sap flux within the tree trunk could be shifted as well as dampened. However, in this study we did not correct for delays or dampening, because we had no estimates for the use of stored stem water or storage capacities over our stem profiles, and sought to avoid adding additional uncertainty by potentially incorrect parameter choice (see Section 4).

The ACASA and STANDFLUX models include interception submodels. Both interception modules indicated a contribution of evaporation from wet surfaces such as needles (E_w) for the first day with similar magnitudes (Fig. 3c). Furthermore, the STANDFLUX model indicated some contribution of E_w until day 265. The difference between E_c measured by eddy-covariance (36 – 2.25 m) and determined with sap flux measurements reached daily maximum values of up to 93 W m^{-2} for 4 of the 5 days, which is about three times larger than the maximum E_w from the two models for the first day. Estimates of E_w on day 263–265 were less than on day 266. However, the large E_w estimates on day 266 (147 W m^{-2}) occurred during turning wind direction, where footprints of above and below canopy eddy-covariance measurements were less comparable than during the other periods.

The soil and understory evapotranspiration ($E_g + E_s$, Fig. 3d) as measured with the eddy-covariance system within the trunk space reached maximum daytime values of 40 W m^{-2}. The ACASA model captured these maximum values, but generally overestimated $E_g + E_s$. The soil module of STANDFLUX underestimated measured daytime $E_g + E_s$ with daily maximums reaching about 30% of the value of the measurements.

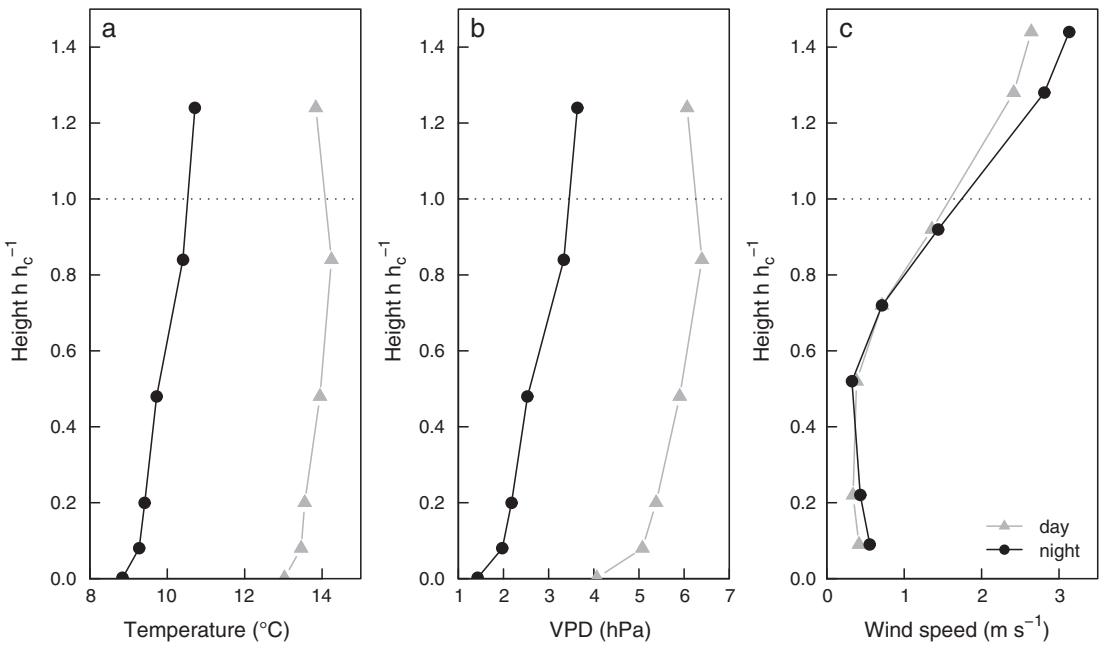

Fig. 2. Comparison of mean daytime and nighttime air temperature (a) and vapor pressure deficit (*vpd*) (b) profiles at the 'main tower' and of mean daytime and nighttime wind speed profiles (c) at the 'turbulence' and 'main tower' (eddy-covariance measurements) for 20–24 September (DOY 263–267).

The coupling regimes were determined mathematically after Thomas and Foken (2007a), with analysis of the distribution of coherent structures within the profile as outlined in Chapter 2.2.1. Decoupled conditions (wave motion and decoupled canopy, Wa and Dc) prevailed during nighttime and partly coupled conditions (decoupled subcanopy, Ds) during daytime (Fig. 3e). Coupled conditions (coupled subcanopy by sweeps and fully coupled subcanopy, Cs and *C*) were not bounded to daytime but were also found during nighttime. These coupling regimes will be used to sort the data later in this study.

Scatter plots in Fig. 4a, b and Fig. 5 illustrate the underestimation of E_c for all systems compared to eddy-covariance estimates during the first 2 days. For the last 3 days, a difference in the scatter plots is seen for the ACASA model and a slight difference for the STANDFLUX model. As indicated by the change in wind direction on the evening of day 265 (Fig. 1g), this could imply a simultaneous change in the footprint area preferentially sampled by the eddy-covariance measurements. Alternatively, the better agreement of modeled and eddy-covariance E_c towards the end of the 5-day-period may indicate that our initial assumption of negligible E_w may not hold for the first days. Meteorological data (Fig. 1) showed a rainy period on day 261, just 2 days before the fair weather period on which this study concentrates. After this rain event, the vapor pressure deficit remained lower for the first few days, which might indicate a wet canopy. Furthermore, the present weather detector (PWD 11, Vaisala) at a height of 24 m at the 'main tower' indicated fog after the rain event on day 261 which lasted until noon of day 262. Thus, the difference of above and in-canopy eddy-covariance measurements might not only represent E_c but also includes E_w. Unfortunately, no independent measurements of canopy interception which would enable the derivation of the contribution of E_w were available for our site. When $E_c + E_w$ as simulated by the two models is compared to eddy-covariance measurements (36–2.25 m), underestimation was slightly reduced and correlation improved (ACASA: $y = 6.4 + 0.76x$, $R^2 = 0.82$; STANDFLUX: $y = -2.56 + 0.82x$, $R^2 = 0.82$). This shows that, although interception needs to be considered in this study, it can only explain a minor part of the discrepancies in E_c obtained through eddy-covariance measurements and models as well as sap flux estimates.

3.3. Canopy evapotranspiration profiles

The models and the sap flux as well as the eddy-covariance measurements allow the study of the partitioning of (evapo-) transpiration within the profile. At the 'turbulence tower' five eddy-covariance systems were positioned within the canopy, and the highest eddy-covariance system was placed 11 m above the canopy at the top of the tower. Unfortunately, there was no system located directly at the canopy top. But assuming a constant flux layer above the canopy as in the ACASA model, the highest system can be taken to represent canopy top measurements and will be displayed as such in the following figures.

For the 5 days mean canopy evapotranspiration profiles were calculated for daytime and nighttime as well as for the coupling regimes as explained above. The investigation of averaged profiles circumvents the variability and thus the limited representativeness of half-hourly eddy-covariance measurement values. A similar approach was employed in a study by Wilson and Meyers (2001) on the spatial variability of subcanopy fluxes at the forest floor, where an averaging time of 4 h (eight samples) to 1 day (48 samples) was suggested to achieve reasonable subcanopy flux data for model validation.

3.3.1. Variability throughout the day

Mean daytime and nighttime profiles of canopy evapotranspiration ($E_c + E_w$) for the two models and the eddy-covariance measurements as well as profiles of canopy transpiration (E_c) from sap flux measurements are displayed in Fig. 6. For sap flux measurements, the mean of the individual error due to the scaling procedure from tree to stand and due to measurement uncertainties is shown for all heights within the profiles (see Appendix for derivation of the error estimates). According to Mauder et al. (2006) the accuracy of latent heat fluxes measured with a type B sonic anemometer (here: USA-1, quality flag 1–6) is 20%. For comparison, the error bar of the values at the uppermost eddy-covariance measurement height is also 20%.

Error measures were calculated by comparing model results and measurements (for all profile levels combined, Tables 4 and 5). Therefore, eddy-covariance measurements at the 'turbulence

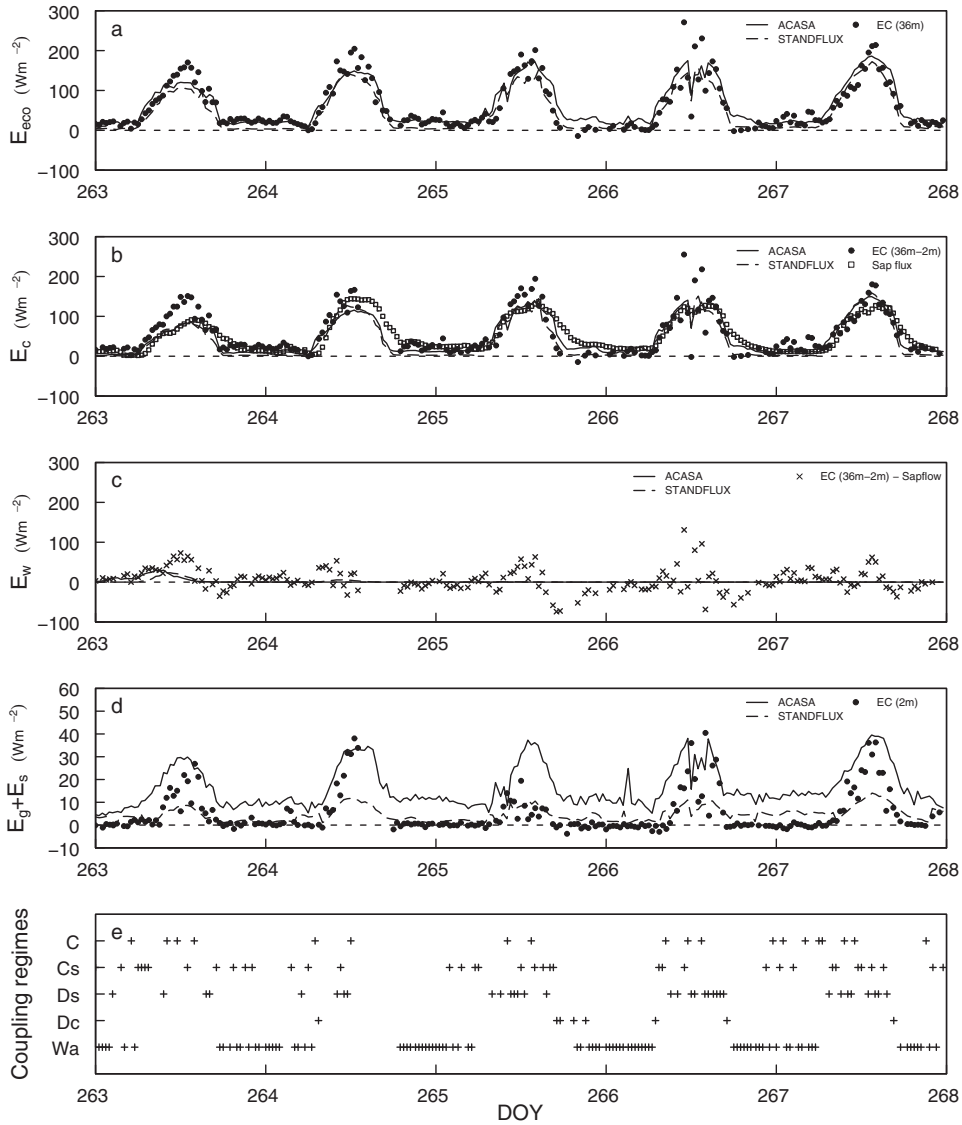

Fig. 3. Ecosystem evaporation (E_{eco}, a) for DOY 263–268 as measured by the eddy-covariance (*EC*) system at 36 m and modeled by ACASA and STANDFLUX. Canopy transpiration (E_c, b) as measured by the eddy-covariance systems (evapotranspiration from the forest floor as measured by the eddy-covariance system at 2.25 m was subtracted from the eddy-covariance measurements at 36 m) and the sap flux measurements; as well as modeled by ACASA and STANDFLUX. Evaporation from interception water (E_w, c) as modeled by ACASA and STANDFLUX. The difference of eddy-covariance measurements at 36 m and the sap flux measurements is shown for comparison. Evapotranspiration from soil and understory ($E_g + E_s$, d). Coupling regimes (e).

Table 4
Error measures for the comparison of day- and nighttime profiles for model results and sap flux measurements compared to eddy-covariance measurements. *MBE*, *MAE* and *RMSE* are expressed as the percentage of the mean canopy top eddy-covariance measurement value (daytime (N = 87): 100 W m^{-2}, nighttime (N = 65): 19 W m^{-2}).

Model/Measurement	*MBE* (%)	*MAE* (%)	*RMSE* (%)	*d*	R^2
Daytime					
ACASA ($E_c + E_w$)	−6.1	17.2	26.8	0.92	0.75
ACASA (E_c)	−7.8	17.2	27.1	0.91	0.75
STANDFLUX ($E_c + E_w$)	−3.6	16.2	25.3	0.93	0.77
STANDFLUX (E_c)	−5.8	16.4	25.7	0.92	0.77
Sap flux measurements (E_c)	−5.2	18.0	27.5	0.91	0.73
Nighttime					
ACASA ($E_c + E_w$)	−24.6	40.2	64.5	0.57	0.28
ACASA (E_c)	−26.7	40.9	65.2	0.56	0.29
STANDFLUX ($E_c + E_w$)	−45.7	50.7	79.6	0.46	0.28
STANDFLUX (E_c)	−45.7	50.7	79.6	0.46	0.28
Sap flux measurements (E_c)	−5.6	45.7	69.1	0.69	0.23

tower' are used as reference values for the comparison of model results and sap flux measurements, which were interpolated for the eddy-covariance measurement heights using a method after Akima (1978) as explained above. Errors are displayed as a percentage of the mean measurement value at canopy top for the respective time period.

Table 5
Error measures for the comparison of day- and nighttime E_c profiles for model results compared to sap flux measurements. *MBE*, *MAE* and *RMSE* are expressed as the percentage of the canopy top sap flux measurement value (daytime (N = 87): 84 W m^{-2}, nighttime (N = 65): 20 W m^{-2}).

Model/measurement	*MBE* (%)	*MAE* (%)	*RMSE* (%)	*d*	R^2
Daytime					
ACASA (E_c)	−3.0	11.5	16.0	0.97	0.91
STANDFLUX (E_c)	−0.7	11.8	17.1	0.97	0.89
Nighttime					
ACASA (E_c)	−19.5	30.7	46.5	0.71	0.67
STANDFLUX (E_c)	−37.1	44.8	65.9	0.47	0.52

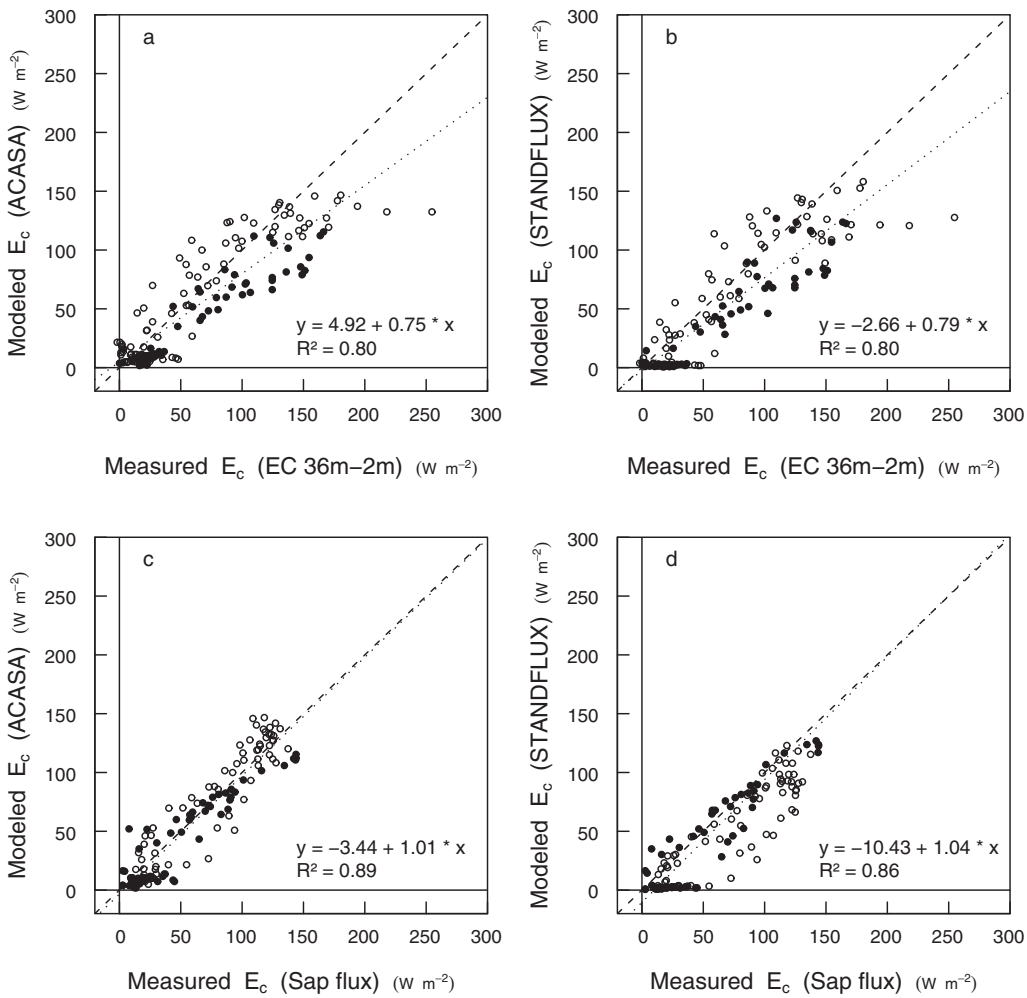

Fig. 4. Scatter plots for the comparison of measurements and models for DOY 263–264 (filled circles) and DOY 265–267 (open circles) ($N = 125$): canopy transpiration (E_c) as modeled with STANDFLUX and ACASA versus measured E_c by eddy-covariance (*EC*, 36–2.25 m) (a) and (b); as well as versus sap flux measurements (c) and (d).

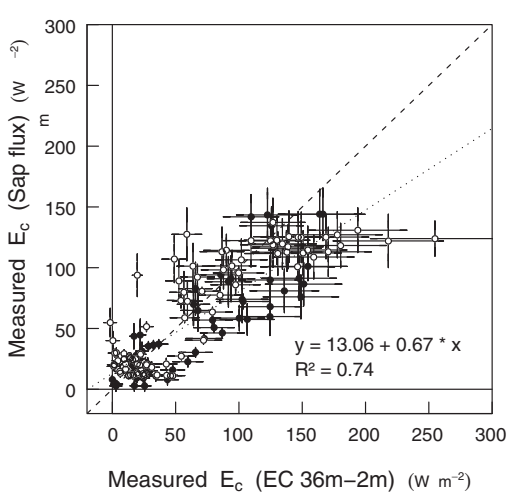

Fig. 5. Scatter plot for the comparison of transpiration (E_c) measured with sap flux versus transpiration (E_c) measured with eddy-covariance (*EC*, 36–2.25 m) with its errors for DOY 263–264 (filled circles) and DOY 265–267 (open circles) ($N = 125$). For the estimation of sap flux errors see explanations in the Appendix. For eddy-covariance measurements, an error of 20% is added to the data for comparison (Mauder et al., 2006).

The E_c profile measured with the sap flux technique resulted in lower values than the $E_c + E_w$ measurements made with eddy-covariance systems for all heights during daytime, with a similar shape as indicated by a R^2 value of 0.73 (Table 4). During nighttime, the sap flux profile had a different shape than the eddy-covariance profile with a low R^2 of 0.23. For most of the canopy with the exception of the uppermost part above $0.8h_c$, sap flux derived measurements were smaller than eddy-covariance data during nighttime.

Mean daytime $E_c + E_w$ profiles of the models agreed well with eddy-covariance measurements (Fig. 6a). Errors were lower than 20% (*MAE*) and the indexes of agreement as well as the R^2 value were high, with only minor differences for the two models (Table 4). Errors are slightly larger when comparing modeled E_c profiles to eddy-covariance profiles. For nighttime, both models underestimated eddy-covariance $E_c + E_w$ profiles, with different performances of the two models (Fig. 6b). For ACASA, errors were smaller with a *MAE* of 40.2% compared to 50.7% for STANDFLUX. Furthermore, the index of agreement was larger than for STANDFLUX. Despite the different degrees of underestimation, both models had a similar but low R^2 (0.28).

Modeled daytime profiles of E_c agreed better with sap flux measurements than with eddy-covariance measurements (in Fig. 6, only $E_c + E_w$ profiles are displayed for the models). Whereas modeled $E_c + E_w$ profile values underestimated eddy-covariance measurements with *MAE* of 17.2% for ACASA and 16.2% for STAND-

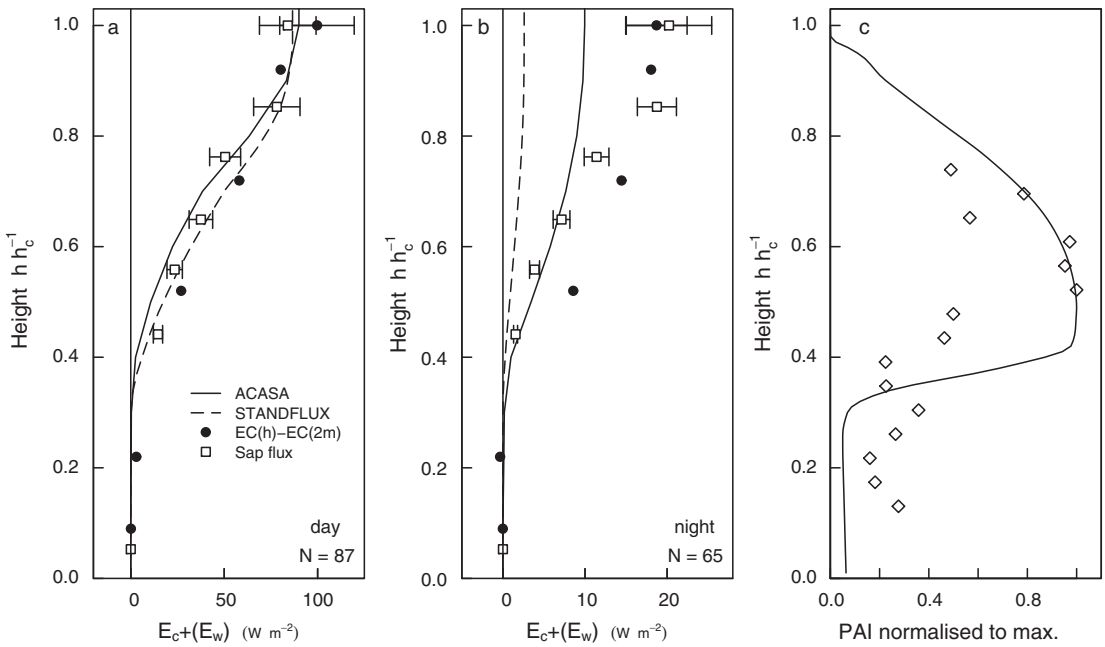

Fig. 6. Comparison of mean daytime (a) and nighttime (b) evapotranspiration ($E_c + E_w$; eddy-covariance measurements (*EC*), ACASA, STANDFLUX) and transpiration profiles (E_c; sap flux). Error estimates are included for sap flux measurements (mean of the individual measurement errors). For eddy-covariance measurements an error of 20% is added to the data of the uppermost height for comparison (Mauder et al., 2006). Note the different ranges of the *x*-axis for daytime and nighttime. Plant area index profile (c) normalized to the maximum value. Diamonds mark measurements made in April 2008, the line represents the *PAI* profile as derived for STANDFLUX and used in ACASA.

FLUX, the underestimation for modeled E_c profiles compared to sap flux profiles was smaller with *MAE* of 11.5% for ACASA and 11.8% for STANDLFUX (Table 5). During nighttime, the different model results deviated from each other, and also had lower profiles than those derived for sap flux. Modeled profile shapes were in better agreement with profile shapes from sap flux measurements (daytime R^2 = 0.91 and 0.89, nighttime R^2 = 0.67 and 0.52, for ACASA and STANDFLUX, respectively). The comparison with eddy-covariance measurements resulted in lower R^2 (daytime: 0.75 and 0.77, respectively, and nighttime: 0.29 and 0.28, respectively).

Estimated mean relative errors for sap flux measurements at canopy top were 18% for daytime and 26% for nighttime. For daytime, mean relative errors of 16–18% for the other measurement heights were similar. During nighttime, the largest errors were estimated for total E_c. Within the canopy, errors were between 13% and 16%.

To obtain a better indication of the model performance during the course of the day, hourly profiles were calculated and errors analyzed with the same method used for daytime and nighttime profiles (Fig. 7). The general picture of a better agreement at daytime than at nighttime is found again. For STANDFLUX the nighttime underestimation is more or less constant during the whole night. Furthermore, evaporation from intercepted water does not seem to play a role during nighttime for STANDFLUX and during the first half of the night for ACASA, as results for E_c and $E_c + E_w$ are the same. For ACASA, there is more variability in performance during nighttime, but still a general underestimation, although less than for STANDFLUX. In the morning hours (8:00), both models have positive *MBE*, thus the onset of evapotranspiration within the profiles took place earlier than in the eddy-covariance measurements. Best agreement with lowest errors and indexes of agreement close to one is achieved just before and at noon. Sap flux measurements also agree better with eddy-covariance measurements during daytime than during nighttime, but with an underestimation during most of the day. Only in the evening hours are profiles measured with the sap flux technique larger than eddy-covariance measurements. The considerable overestimation in the early evening (19:00 and 20:00) suggested a time shift in sap flux data compared to eddy-covariance data. But due to the low number of profiles for averaging and highest stability with very low fluxes measured by eddy-covariance at this time of the day, this feature has to be viewed with caution.

The measured and modeled evapotranspiration profiles allow the calculation of the contribution of the canopy layers to total canopy evapotranspiration. These were determined for 10 equally spaced layers and for each measurement system or model separately (Fig. 8). During daytime, contributions of the two models peaked at $0.75h_c$ (STANDFLUX 25%, ACASA 27%), and the sap flux measurements at $0.75 - 0.85h_c$ (22% and 23%). Eddy-covariance measurements had maximum contributions for the uppermost layer and at $0.65h_c$. Both measurements indicated some contributions of the lowest third of the canopy, whereas model contributions came from only the upper two thirds of the canopy. The results of the two models indicated that the contribution of evaporation from intercepted water came from the mid-canopy, which was still wet during the first day of the 5-day study period. Contributions during nighttime shifted downward in the canopy for eddy-covariance measurements and the two models, with less pronounced peaks at $0.55h_c$ for STANDFLUX and $0.45h_c$ for ACASA. For eddy-covariance measurements, all layers between 0.2 and $0.8h_c$ accounted nearly equally to $E_c + E_w$. Only the sap flux measurements still had a peak at $0.75h_c - 0.85h_c$, with only a small shift in the contributions towards the lower layers. While ACASA showed some contribution of evaporation from intercepted water from the mid-canopy, there was no contribution of E_w in STANDFLUX simulations.

3.3.2. Coupling stages

Profiles were not only sorted for different times of the day but also for the coupling regimes that were calculated from the vertical distribution of coherent structures after Thomas and Foken (2007a, Fig. 3c). Due to the uneven distribution of half-hourly values amongst the coupling stages, the five classes were combined to only three classes: coupled conditions for coupled subcanopy by

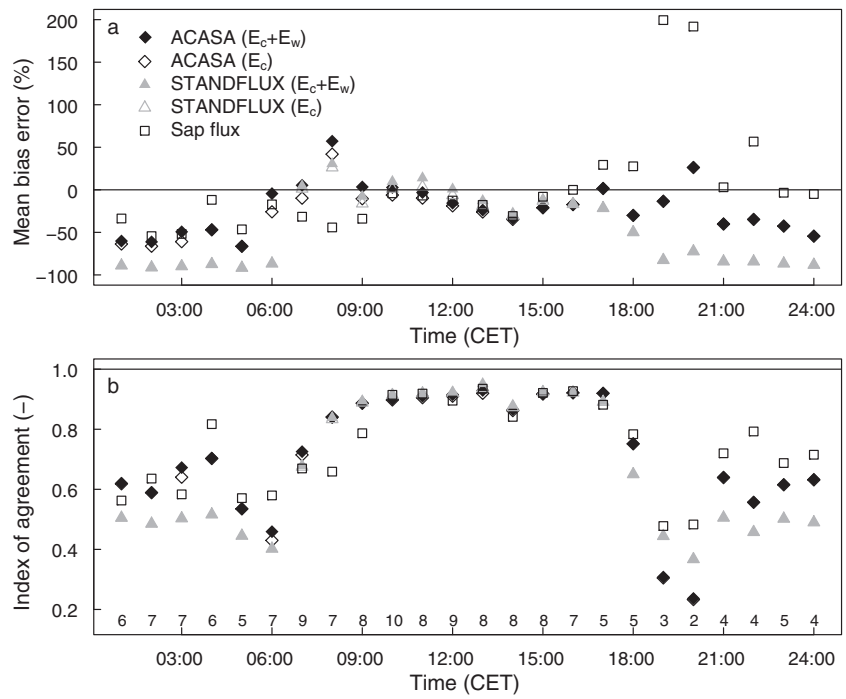

Fig. 7. Error measures comparing hourly canopy transpiration (E_c) and canopy evapotranspiration ($E_c + E_w$) profiles to eddy-covariance data: mean bias error (*MBE*, a) expressed as percentage of the mean canopy top eddy-covariance measurement value and index of agreement (*d*, b). The numbers at the baseline in plot (b) indicate the number of half-hourly profiles used for calculating error measures (10 is the maximum available number, fewer profiles result either from instrument failure or quality filtering for eddy-covariance data). Note that the symbols are on top of each other for $E_c + E_w$ and E_c for STANDFLUX and ACASA during most of the nighttime hours.

sweeps and fully coupled subcanopy (Cs and *C*), partly coupled conditions for decoupled subcanopy (Ds) and decoupled conditions for wave motion and decoupled canopy (Wa and Dc).

The models were able to capture $E_c + E_w$ for partly coupled and coupled situations well, whereas modeled fluxes were too low throughout the profile for decoupled situations (Fig. 9). Overall model agreement was best for partly coupled situations with lowest errors (*MAE*: ACASA 17.2%, STANDFLUX 16.4%) and largest indexes of agreement (ACASA 0.93, STANDFLUX 0.94, Table 6). For this coupling stage the mean total $E_c + E_w$ was largest due to the distribution of decoupled situations during the course of the day, with mainly daytime values. On the other hand, decoupled conditions were mainly detected during nighttime, thus the results closely resemble those during nighttime, with better results for ACASA than for STANDFLUX (*MAE*: ACASA 39.6%, STANDFLUX 47.6%). Only coupled situations were not restricted to any time of the day, thus the mean total $E_c + E_w$ is lower than for daytime and partly coupled situations and larger than for nighttime and decoupled situations. Errors were larger than for partly coupled situations with an underestimation of measured values (*MAE*: ACASA 18.9%, STANDFLUX 18.9%), but both models performed equally well. Performance of both models was slightly worse when E_c profiles were compared to eddy-covariance measurements during all coupling situations for both models, thus the taking of E_w into account increased agreement.

Again, sap flux measurements resulted in lower E_c rates throughout the profile compared to eddy-covariance measurements for coupled conditions, and only slightly lower values for partly coupled conditions. Agreement was also best for partly coupled situations (*MAE*: 17.6%, *d*: 0.92, Table 6). For decoupled conditions, the shape of the profile was again different for sap flux measurements when compared to eddy-covariance measurements with an overestimation in the uppermost part of the canopy but an underestimation in the middle part of the canopy. This resulted in a very low, positive *MBE* of 2.2% and a *MAE* of 49.1%. Decoupled conditions not only occured during nighttime, but also in the evening hours when the delay in sap flux measurements compared to eddy-covariance measurements was most obvious.

Table 6
Error measures for the comparison of mean profiles for model results and sap flux measurements compared to eddy-covariance measurements for the three coupling situations. *MBE*, *MAE* and *RMSE* are expressed as the percentage of the mean canopy top eddy-covariance measurement value (Wa/Dc (N = 51): 20 W m^{-2}, Ds (N = 27): 104 W m^{-2}, *C*/Cs (N = 41): 80 W m^{-2}).

Model/Measurement	*MBE* (%)	*MAE* (%)	*RMSE* (%)	*d*	R^2
Wa/Dc					
ACASA ($E_c + E_w$)	−15.9	39.6	64.1	0.64	0.23
ACASA (E_c)	−17.1	40.2	64.6	0.64	0.23
STANDFLUX ($E_c + E_w$)	−35.6	47.6	75.6	0.52	0.10
STANDFLUX (E_c)	−35.7	47.6	75.6	0.52	0.10
Sap flux measurements (E_c)	2.2	49.1	75.5	0.69	0.24
Ds					
ACASA ($E_c + E_w$)	−4.2	17.2	24.3	0.93	0.75
ACASA (E_c)	−5.0	17.2	24.3	0.93	0.76
STANDFLUX ($E_c + E_w$)	−1.8	16.4	23.0	0.94	0.77
STANDFLUX (E_c)	−2.9	16.0	22.7	0.94	0.78
Sap flux measurements (E_c)	−0.4	17.6	25.0	0.92	0.73
C/Cs					
ACASA ($E_c + E_w$)	−11.9	18.9	34.0	0.91	0.79
ACASA (E_c)	−13.6	18.7	34.3	0.91	0.80
STANDFLUX ($E_c + E_w$)	−11.5	18.9	33.3	0.92	0.79
STANDFLUX (E_c)	−13.2	19.2	33.5	0.92	0.80
Sap flux measurements (E_c)	−10.9	19.2	34.4	0.91	0.79

4. Discussion

4.1. Measurements of canopy transpiration

Transpiration of the canopy (E_c) could be determined from the difference of eddy-covariance measurements above the canopy and above the forest floor and from sap flux measurements. For the

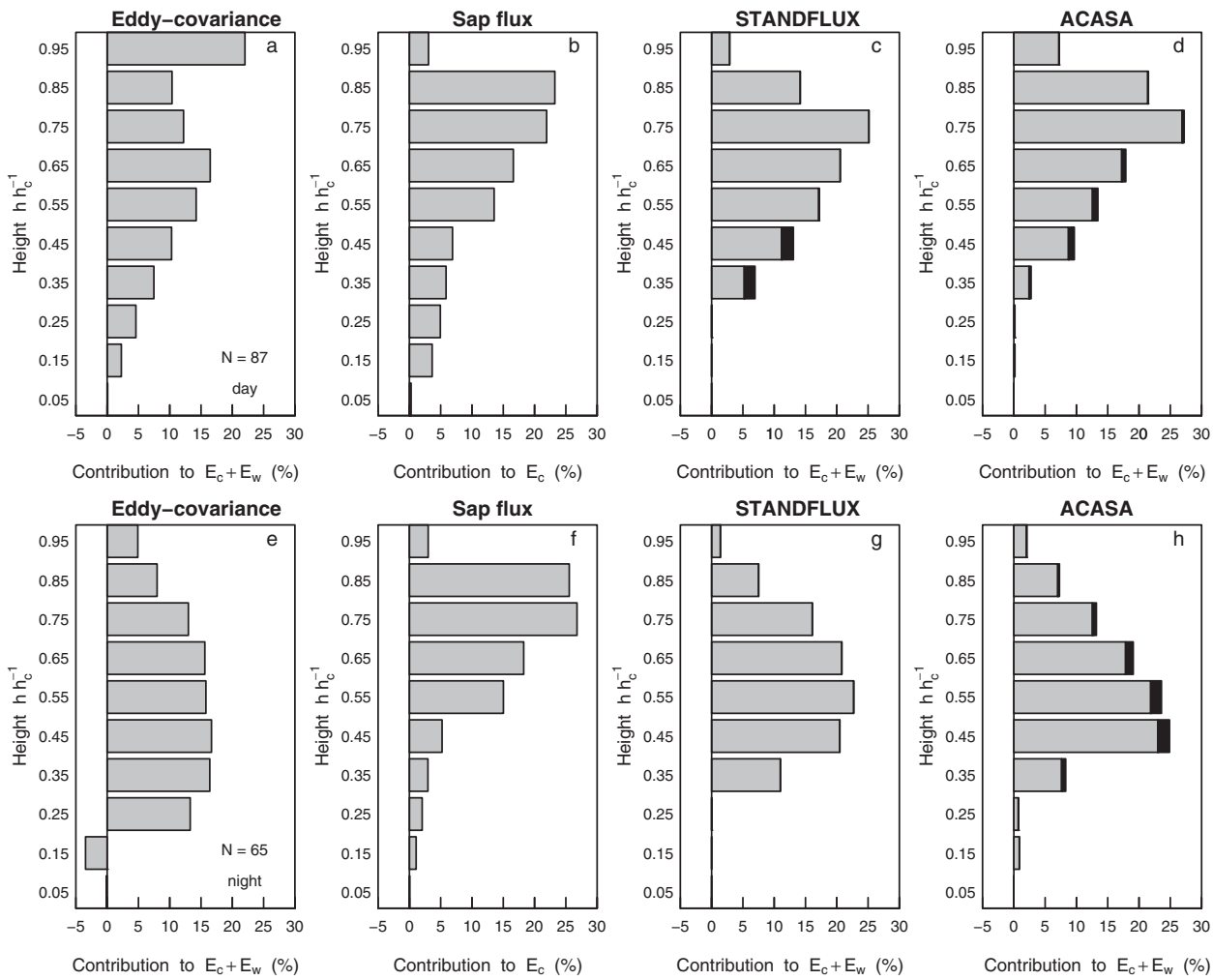

Fig. 8. Partitioning of canopy evapotranspiration ($E_c + E_w$) for equally spaced layers within the canopy for daytime (a)–(d) and nighttime (e)–(h). For ACASA and STANDFLUX, the contribution of canopy evaporation (E_w) is highlighted in black. Values at the *y*-axis indicate the middle of the layer.

whole study period, E_c from sap flux measurements was lower than determined from eddy-covariance measurements for most of the day with the exception of the evening hours (Fig. 3, Table 3). This same discrepancy between the different measurement systems with lower estimates for sap flux measurements was observed at several sites for example during dry periods at a semi-arid forest (Yaseef et al., 2009). At mixed deciduous forests, Wilson et al. (2001) reported lower transpiration estimates for sap flux measurements than for eddy-covariance measurements at the annual and daily time scale, whereas Oishi et al. (2008) only found larger values for evapotranspiration estimated from its components, including sap flux measurements, than for the direct measurements with the eddy-covariance system for periods with very high radiation loads. Several reasons for such discrepancies have been proposed in the literature and will be discussed in the following for our site.

One reason suggested was the inaccurate assessment of the components of evapotranspiration (Granier et al., 2000; Oishi et al., 2008). The application of the eddy-covariance technique requires knowledge of the underlying assumptions and the performance of a series of corrections and quality checks to achieve reasonable flux data (Mauder et al., 2006). Nevertheless, the unclosed energy balance that is observed at many forest sites of approximately 80% (Aubinet et al., 2000; 81% for EGER IOP-1, Foken et al., in preparation) even after thorough analysis and filtering of flux data, indicates an underestimation of sensible and latent heat fluxes, probably due to the contribution of larger eddies caused by the heterogeneity of the landscape (Foken, 2008). But this situation would lead to an amplification of the mismatch between E_c measurements using the eddy-covariance and the sap flux techniques rather than serving as an explanation for this discrepancy.

As E_c from eddy-covariance measurements was calculated as the difference between above canopy and above forest floor measurements, an underestimation of the forest floor measurements, and thus an underestimation of soil and understory evapotranspiration ($E_g + E_s$), could lead to E_c rates that are too large. The reliability of eddy-covariance measurements in the canopy may be questioned due to the limitations of the underlying assumptions. Several studies analyzing eddy-covariance measurements above the canopy and in the trunk space of a forest proved the reliability of in-canopy measurements by analyzing the energy balance closure in the trunk space and spectral analysis (Baldocchi et al., 2000; Roupsard et al., 2006). Wilson et al. (2000) estimated that $E_g + E_s$ measured by an eddy-covariance system was about 10% too low due to high frequency loss on an annual time scale. But as maximum daytime $E_g + E_s$ only reached magnitudes of up to 40 W m^{-2} (Fig. 3d), a 10% underestimation is very little compared to the differences of E_c measured by eddy-covariance and sap flux (Fig. 3c) and can not explain these.

In our case, even though a fair weather period prevailed, evaporation from intercepted water (E_w) could not be excluded as a possible explanation for the mismatch. Unfortunately, no interception measurements were available, but a rain event 2 days before

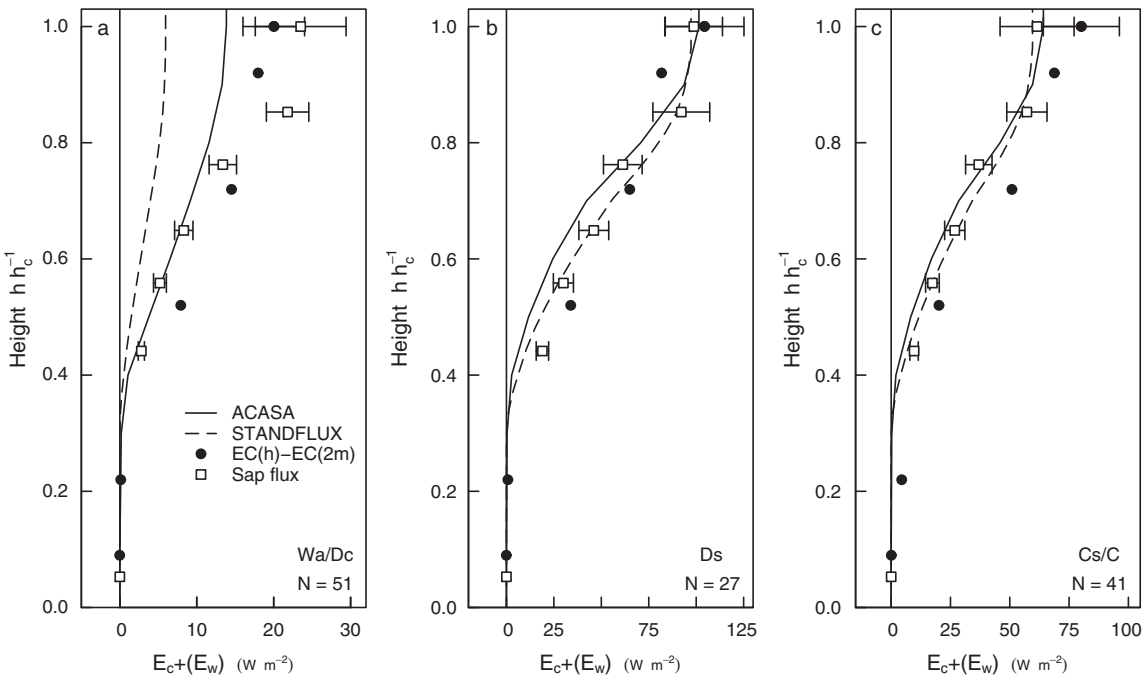

Fig. 9. Comparison of mean evapotranspiration ($E_c + E_w$; eddy-covariance measurements (*EC*), ACASA, STANDFLUX) and transpiration profiles (E_c; sap flux) for decoupled (a), partly coupled (b) and coupled (c) situations. Error estimates are included for sap flux measurements (mean of the individual measurement errors). For eddy-covariance measurements an error of 20% is added to the data of the uppermost height for comparison (Mauder et al., 2006). Note the different ranges of the *x*-axis for the three coupling regimes.

the study period could be a possible influence (Fig. 1). Such a contribution of evaporation from intercepted water 2 days after the rainfall event would be exceptional; for example, Czikowsky and Fitzjarrald (2009) detected evaporation from intercepted water from eddy-covariance measurements in a tropical rainforest only during the day of rainfall or the day after rainfall when rainfall occurred at night. At the Waldstein–Weidenbrunnen site, fog frequently occurs on about 200 days per year on average (1997–2001, Klemm and Wrzesinsky, 2007). The fog detected after the rain event on day 261 until noon of day 262 probably prevented evaporation from intercepted water, delaying evaporation from the interception pool. The difference between sap flux and eddy-covariance measurements had nearly the same daily cycle for the whole period with similar maximum daily differences (up to 100 W m^{-2}, Fig. 3c). If E_w was the main reason for the mismatch, we would expect decreasing differences over the study period due to a drying canopy under fair weather conditions. Thus, E_w might have played a role during the first days, as indicated by the model simulations (Fig. 3c), but only to a smaller extent than the mismatch between the two measurement systems. Rather, the change in wind direction on the evening of day 265 and the associated change in the footprint area of the eddy-covariance measurements might explain the better agreement of eddy-covariance and sap flux measurements during the last 3 days (Fig. 4). This issue will be discussed below in more detail.

Scaling sap flux measurements from tree to stand was done thoroughly, but still involved several uncertainties. Gaussian propagation of uncertainties of the scaling parameters was performed (see Appendix), and revealed a daytime maximum uncertainty for half-hourly estimates of scaled sap flux measurements of 22 W m^{-2} (15%) (slightly lower than eddy-covariance estimates with 20%; Mauder et al., 2006). Nighttime uncertainties might become as high as 5 W m^{-2} (250%), but absolute fluxes were much lower at night. These large uncertainty estimates are not surprising given the large uncertainties of the various scaling parameters and their propagation (see Appendix). The mean absolute error between E_c from eddy-covariance and sap flux is larger (30 W m^{-2} during day, 13 W m^{-2} at night, Table 3) than the uncertainty of the sap flow estimates. That is, the difference between eddy-covariance and sap flux estimates exceeds the accuracy of the sap flux estimates.

The uncertainty estimates for the sap flux estimates of E_c here included the variation among sensor readings, the uncertainties in determining sap flux area, representativeness of sample trees, and tree quantity. The error of time lags and dampening effects between transpiration and sap flux, due to water recharge in the stems (e.g. Schulze et al., 1985) or in the upper canopy (Oishi et al., 2008) was not considered (however, this aspect is discussed below).

With respect to among tree variability, Köstner et al. (1996) estimated that a measurement error of at least ±8% is caused by among tree variability. For temperate forests, Granier et al. (1996) reported coefficients of variation of individual sap flux readings of 10–15%, both results being close to our estimates of 12% for the outer and 11% for inner thermocouple readings. Reports of higher errors might include seasonal variability, drought effects, or species sampled (Oren et al., 1998), whereas in our case five well-watered days in early autumn were analyzed. For example, Köstner (1999) found a maximum error of 18–23% for a 140 year-old *P. abies* stand adjacent of the Waldstein–Weidenbrunnen site; Granier et al. (1996) reported 35–50% in tropical forests. Close to our values due to among tree variability is the uncertainty of ca. 10% introduced by sap wood area estimates. It is mainly introduced by the measurement uncertainty of sapwood depth with a coefficient of variation of 13%. The error associated with sapwood area estimates is low compared to other publications: values of 15–29% are reported by Phillips et al. (2002) for estimates of sapwood depth for Douglas fir trees. Uncertainties due to the representativeness of sample trees *S* were again of similar magnitude as the other errors in our study (with averages of 8–15% for the inner sapwood ring and 9–20% for the outer sapwood ring). Comparison of these values with other studies is difficult, because we did not directly use sapwood area to scale from tree to stand, but representativeness of the two sample trees with respect to the scaled flux as described in

Section 2.2.2. The largest contribution to total uncertainty in the study here was due to the uncertainty of tree quantity (N), the number of trees per m^2, a number typically assumed to be a fixed quantity. In our study uncertainty of N is caused by the high spatial variation in N in the investigated area, especially when extended to an area that covers potential footprint areas of individual eddy-covariance data. Overall the contribution of representativeness of sampling trees and tree quantity to the total error is much larger than that of among tree variability and individual sap wood area estimates. The contribution of the error of scaled inner (or outer) sensor readings to the total error amounted to 4–79% (96–21%), basically reflecting the ratio between inner (or outer) sapwood areas to total sapwood area. The large variability here resulted from different contributions at the six installation heights, with the largest contribution of the inner ring to total sapwood area at the trunk installation.

The relationship between E_c estimates from eddy-covariance and sap flux showed hysteresis effects (see Fig. 7), caused by the delaying and dampening of sap flux signals compared to eddy-covariance data. Time lags between transpiration in the tree canopy and sap flux observation in the stem have been studied over the last four decades (e.g. Lassoie et al., 1977; Schulze et al., 1985; Hatton and Vertessy, 1990; Köstner et al., 1992, 1998; Granier and Loustau, 1994; Phillips et al., 1997; Lundblad and Lindroth, 2002; Kumagai et al., 2009). Time lags are interpreted as the time necessary for the sapwood at installation height to equilibrate with the evaporative demand in the canopy. Recently, Oishi et al. (2008) discussed nocturnal fluxes being caused by the recharge of water to upper trunks and branches as well as nocturnal water loss. To account for the time lag, correlation analyses between eddy correlation data and stem sap flow data, for example, could be performed. However, the analyses reported in Phillips et al. (1997) suggest that using eddy correlation data may not be useful for determining time lags, because correlation at lags from −1.0 to +0.7 h were not significantly different from correlation at zero lag. This might be caused by the long averaging intervals (20 min in Phillips et al., 1997; 30 min averaging intervals used for both techniques in our study), and uncertainties associated with either technique. In contrast, Lundblad and Lindroth (2002) determined time lags from 1 to 2.5 h between eddy-covariance and sap flux time series when fitting to the Penman–Monteith equation inverted for canopy conductance, and explained 50–75% of the variations in-canopy conductance for the calibration period. As an alternative to the correction for the time lag and dampening of the sap flux signal, parameters for water storage capacity and hydraulic conductivity for the different compartments of the investigated trees could have been calibrated using the measured eddy-covariance and sap flux times series. However, time resolution and uncertainty of those data again discouraged trials to account for the time lag and dampening of the sap flux signals in this analysis.

Radial trends in sap flux readings for tree species of different wood anatomy were observed in a series of studies (e.g., Phillips et al., 1996; Cermak and Nadezhdina, 1998; Wullschleger and King, 2000; Nadezhdina et al., 2002; Ford et al., 2004; Kumagai et al., 2005; Poyatos et al., 2007; Oishi et al., 2008; Caylor and Dragoni, 2009). Extrapolation from the sensor readings at different radial depths to the entire xylem is then performed employing linear, quadratic or Gaussian functions. In this study sap flux sensor readings were extrapolated to the entire xylem based on a linear approach, with simple summation of sapwood area weighted individual values, to minimize additional uncertainties introduced by prescribing more complex functions. The ratio between inner and outer sap flux readings (f, m s^{-1}) for our trees increased with increasing circumference at installation height ($f_i/f_o = 0.46\ ln(CH) + 1.28$, $R^2 = 0.81$), consistent with the findings of other studies (Phillips et al., 2002; Wullschleger and Norby, 2001). However, average ratios of $f_i/f_o = 1$ were already reached for CBH of 0.54 m, much lower values than reported in Phillips et al. (2002).

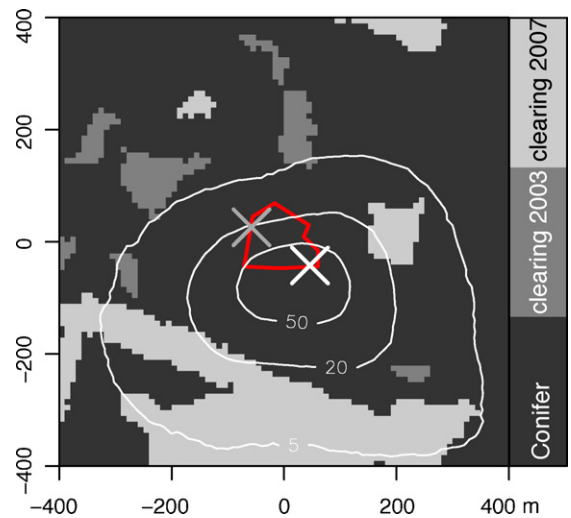

Fig. 10. Footprint climatology over land use map for EGER IOP-1 (19 September–8 October 2007) for the eddy-covariance measurement at the top of the 'turbulence tower' after Siebicke (2008) (no distinction for stratification was made). White isolines show the relative flux contribution of the corresponding footprint area, with the outermost isoline indicating that only 5% of the flux is coming from the area outside. The white cross marks the position of the 'turbulence tower', the gray cross the position of the 'bio tower'. The red line shows the fenced area where plant morphological measurements were performed and which was used to upscale the sap flux measurements. (For interpretation of the references to color in this figure legend, the reader is referred to the web version of the article.)

In the literature, scaling flux measurements from single tree readings to the entire stand have been performed by a suite of different scalars, for example stem circumference or diameter at breast height, crown projected area, leaf area, basal area, sapwood area, etc. (see review by Wullschleger et al., 1998). If we use circumference at breast height (CBH), needle area, crown projected area (CPA), or CPA multiplied by crown length instead of sapwood area (A_s) and tree representativity (S), our E_c estimates over the 5 days change on average by +29%, −12.5%, +6.1%, and −13.8%, respectively. With the exception of scaling by CBH, the different methods resulted in fluxes similar to those presented in this study. In comparison to the studies by Vertessy et al. (1995) and Hatton et al. (1995), scaling by circumference at breast height performed worse than the other three scaling methods, most likely because at our site basal area is dominated by non-conducting heartwood. As found by Hatton et al. (1995), a measure of tree domain based on distances between stems performed worst: scaling E_c by the polyangular area occupied by the tree (vertices defined by half the distance to the 6–8 nearest neighbour trees) resulted in E_c estimates which were 41.9% larger. The average E_c calculated employing the four scalars (CBH, needle area, CPA, and CPA multiplied by crown length) overestimate E_c presented in this study by only 2.2%. Hence, E_c scaled by sap wood area, and tree representativity (based on a sample of seven trees stratified by CBH) represents a robust estimate of the canopy transpiration at our site.

Plant morphological measurements used to upscale sap flux measurements to the forest stand were performed within a 1.23 ha fenced area (Fig. 10). The footprint area for the upper-most measuring height of the 'turbulence tower' (white isolines in Fig. 10 calculated by Siebicke, 2008, using the methodology described in Göckede et al., 2008) comprises this fenced area, but is much larger. 80% of the footprint covers mainly conifer forest, but the outer 20% of the footprint indicates contributions of clearings to the south and the east of the study site. A comparison of flux measurements at the clearing east of the study site to flux measurements at the

Table 7
Error measures for the comparison of time series for E_c compared to sap flux measurements (Fig. 3b). *MBE*, *MAE* and *RMSE* are expressed as the percentage of the mean canopy top sap flux measurement value (daytime (N = 87): 84 W m^{-2}, nighttime (N = 65): 20 W m^{-2}).

Model/measurement	*MBE* (%)	*MAE* (%)	*RMSE* (%)	*d*	R^2
Daytime					
ACASA (E_c)	3.4	17.1	20.9	0.94	0.80
STANDFLUX (E_c)	−0.8	18.3	23.9	0.93	0.75
Nighttime					
ACASA (E_c)	−54.2	54.8	71.0	0.57	0.54
STANDFLUX (E_c)	−87.2	87.2	103.4	0.43	0.31

'turbulence tower' revealed that the Bowen ratio ($Bo = H/LE$, with the sensible heat flux H and the latent heat flux LE) at the clearing is lower than for the forest, thus the clearing acts as a source of moisture (Foken et al., in preparation). Therefore, especially during periods with southerly wind directions, as occurred for the first 3 days of the studied period, the contribution of the clearings can lead to evapotranspiration rates that are larger than would be found for an area completely covered by spruce forest. In contrast to the area used for upscaling of sap flux measurements, the eddy-covariance footprint is dynamic with different footprints for every 30-min measurement depending on stability and wind direction. Oishi et al. (2008) showed for a mixed forest that the canopy transpiration calculated from sap flux measurements depends largely on the area used for upscaling. For our study, we found the largest contribution to total uncertainty of the sap flux measurements was due to the uncertainty of tree quantity (N), the number of trees per m^2. Thus, the differences between the flux footprint area and the fenced area used to scale up the sap flux measurements could explain differences in canopy evapotranspiration rates for these two techniques.

Comparisons of in-canopy measurements of E_c also revealed an underestimation of eddy-covariance derived $E_c + E_w$ profiles by sap flux measurements. Concerning eddy-covariance profile measurements, the differences of flux footprints of in-canopy measurements have to be additionally considered, with decreasing flux footprints with lower measurement height within the canopy as compared to above canopy flux footprints (Baldocchi, 1997).

4.2. Model – measurement comparisons

Both models underestimated E_c and E_{eco} measured with the eddy-covariance technique. The deviating areas of the flux footprint and the areas represented in the models or used to measure model parameters might also contribute to these differences, as also discussed by Davi et al. (2005) concerning CO_2 fluxes. While the 3D-model STANDFLUX represents all trees within the fenced area of the Waldstein–Weidenbrunnen site and calculates the exchange rates for each tree individually, the ACASA model assumes an area of about 10^4–10^6 m^2, which is a similar size to the flux footprint but is covered by a uniform forest characterized by the plant morphological input parameters such as the *LAI* and its profile derived for the fenced area. Thus, neither the STANDFLUX model nor the ACASA model includes the contributions of clearings, which must be assumed to play a role for the fluxes measured with the eddy-covariance technique. As the areas represented in the models resemble the area used to upscale sap flux measurements, agreement of modeled E_c with sap flux measurements was better (Table 7).

Including E_w in model results when making comparisons to eddy-covariance derived $E_c + E_w$ increased agreement, even though models still underestimated measured $E_c + E_w$. Both models indicated a contribution of E_w for the first 2 days. But whether the interception submodels simulated realistic estimates of E_w needs to be evaluated against interception measurements, which were not available for our experiment.

While the simulations of $E_g + E_s$ of the ACASA model overestimated eddy-covariance measurements at most times of the day, the STANDFLUX model underestimated $E_g + E_s$. The lower $E_g + E_s$ in STANDFLUX can explain the lower E_{eco} than that modeled with ACASA, as modeled E_c and E_w rates were similar in the two models.

The comparison of measured and modeled profiles of E_c and $E_c + E_w$ revealed differences in agreement for the various systems as well as for different times of the day and different coupling regimes. Furthermore, agreement of measured profiles with the eddy-covariance technique and modeled profiles was better when evaporation E_w was included in the comparisons. Both models proved to be able to reproduce mean daytime $E_c + E_w$ profiles well (Fig. 6), with similar results for STANDFLUX and ACASA. For nighttime, the agreement was not as good as for daytime, with ACASA performing better than STANDFLUX. But for the comparisons of nighttime profiles, the lower absolute fluxes should be kept in mind, with the mean absolute value at canopy top of only 20% of the daytime value. Sorting profiles for the different coupling regimes allows assessment of the ability to reproduce evapotranspiration profiles by the two models for different states of turbulent transport of the canopy. Even though best agreement of models and measurements was found for partly coupled situations, differences to coupled conditions are small and might, most likely, stem from the distribution of coupling stages throughout the day, with only daytime values for partly coupled conditions and daytime as well as nighttime values for coupled conditions. The canopy and the atmosphere are coupled for these conditions, which is where the exchange of water occurs within the canopy. The subcanopy, which is the trunk space of the forest, did not contribute much to canopy evapotranspiration, thus no difference in model performance was observed whether the subcanopy was coupled or not. Only for decoupled conditions are errors of the models larger with considerable underestimations. The class of decoupled conditions is mainly made up of situations classified as 'wave motion', which were mainly detected at nighttime and are associated with very low fluxes. The models were not able to correctly predict the profiles of canopy evapotranspiration under such decoupled conditions.

4.3. Partitioning of evapotranspiration

During daytime, $E_g + E_s$ accounts for 10% of E_{eco} measured above the canopy at 36 m (Fig. 3). The contribution of $E_g + E_s$ to E_{eco} within the models was quite different, with a 20% contribution in ACASA and a 7% contribution in STANDFLUX. Compared to the contribution of $E_g + E_s$ as found in other studies at coniferous forests, a measured contribution of 10% is quite low. Baldocchi and Vogel (1996) found a contribution of 50% of $E_g + E_s$ for a boreal conifer forest during summer, Jarosz et al. (2008) an annual contribution of 38% for a maritime pine forest and Kurpius et al. (2003) a contribution of 47% during summer and fall for a ponderosa pine forest. But these forests had a smaller *LAI* (around 3, 2.4 and 2.2, respectively) than measured at our site (*LAI* = 4.8 m^2 m^{-2}, calculated from *PAI* measurements and inventory data). Thus, the available energy in the trunk space was larger, resulting in a higher evapotranspiration rate. But compared to a temperate deciduous forest, the contribution of $E_g + E_s$ at our site is well within the range found for the growing season (Wilson et al., 2000; Baldocchi and Vogel, 1996).

The assessment of the contributions of the canopy layers to E_c showed a maximum within the upper half of the canopy for measurements and models for daytime (Fig. 8). These upper layers above the maximum of the *LAI* contribute about 80%. This part of the canopy is where the largest radiative input and thus the highest radiation absorption occurs, causing larger air and leaf sur-

face temperatures and higher vapor pressure deficits than in the lower part of the canopy during daytime (Fig. 2). Model simulations with SVAT-models incorporating higher order closure turbulence modules indicated similar distributions of water vapor fluxes, with the maximum source strength within the top 30% of the canopy for a broad-leaved forest (Park and Hattori, 2004) and a pine forest (Juang et al., 2008). For these forests, the maximum in the *LAI* profile was at about $0.7h_c$, which is higher than for our site, explaining the contribution of larger parts of the canopy for our site. Unfortunately, comparisons to profile measurements for these sites were not reported. At nighttime, the lower part of the canopy ($0.2 - 0.6h_c$) contributed more to the flux than during daytime for all systems except the sap flux measurements. However, keeping in mind the measurement uncertainties as explained above and the low total nighttime value of 20 W m^{-2} that was distributed within the profile, the differences between the two measurement systems were small. The profiles of the modeled contributions of the canopy layers to E_c at nighttime have a profile shape similar to the *PAI* profile. Thus, at nighttime, the contribution of the layers is proportional to the fraction of *PAI* of the respective layers, whereas at daytime the layers higher up in the canopy contributed more per fraction of *PAI* than the lower layers due to the higher vapor pressure deficits and higher air temperatures of the upper part of the canopy.

5. Conclusions

A detailed study of evapotranspiration of a forest ecosystem including controlling processes and partitioning into its components make a range of measurements within and above the canopy necessary. Furthermore, for the validation of processes determining the components of ecosystem evapotranspiration within complex process-based models, accurate measurements of all components are needed. Here, for a case study of 5 days, a combination of eddy-covariance and sap flux measurements to distinguish all components of ecosystem evapotranspiration was presented and compared to ACASA and STANDFLUX model results.

Even though a good correlation of canopy transpiration measurements using the sap flux technique and differences of eddy-covariance measurements above the forest and in the trunk space was observed, transpiration rates determined by sap flux measurements underestimated the values measured with the eddy-covariance technique. These differences were probably caused by an interplay of several processes, such as uncertainties in the measurement techniques, and different sizes and forest structures in the eddy-covariance flux footprint and the area used to scale sap flux measurements. Furthermore, the assumption of a negligible contribution of canopy evapotranspiration from intercepted water did not hold true. The relative importance of each of these processes could not be determined. Further work should concentrate on these issues, for example by measuring canopy interception and assessing its relative importance, and by studying a longer time period that encompasses more variability in meteorological conditions.

Eddy-covariance measurements within and above the forest canopy gave insights into the partitioning of ecosystem evapotranspiration, the most important component of the water budget of many forests. At the studied spruce forest site, soil and understory evapotranspiration contributed only 10% to ecosystem evapotranspiration during the 5-day study period in fall 2007. The contribution of evaporation from intercepted water was assumed to be minor, even though this point has to be investigated further by direct measurements of canopy interception, as mentioned above. The bulk of ecosystem evapotranspiration was made up of canopy transpiration. Thereby, the upper half of the canopy with 66% of leaf area contributed up to 80% to canopy transpiration at daytime due to the higher air temperatures and higher vapor pressure deficits in the upper part of the canopy.

Not only comparisons of measured and modeled ecosystem evapotranspiration but also its components were performed to achieve more confidence in the ACASA and STANDFLUX models. Keeping the uncertainties of the measurements in mind, both models reflected the contributions of the components of ecosystem evapotranspiration during daytime well. Nighttime discrepancies were larger.

Profile measurements also made it possible to assess the partitioning of canopy evapotranspiration within the canopy. A comparison of mean profiles for daytime and nighttime as well as for three coupling conditions revealed a good agreement of vertical partitioning of canopy evapotranspiration between models and measurements for mean daytime profiles and for partly coupled and coupled situations. For these conditions, the ACASA and the STANDFLUX models performed equally well. During nighttime and for decoupled conditions, both models had problems in reproducing measured profiles, with larger deviations than for daytime conditions.

Altogether, the ACASA and STANDFLUX models proved to be valuable tools to simulate the water exchange of our forest not only as a whole but also its vertical partitioning within the canopy. The ability of the two models to reproduce measurements of the vertical distribution of the components of evapotranspiration depends on the time of the day and the coupling condition of the canopy, with better performance for daytime and a coupled and partly coupled canopy than for nighttime and a decoupled canopy. Despite the differences in model setup, i.e. a three-dimensional representation of the stand in STANDFLUX and the one-dimensional setup of ACASA, the models performed similarly during daytime. Thus, the better representation of turbulence by ACASA with a third-order closure method did not seem to be an advantage when compared to the STANDFLUX model.

Acknowledgments

The authors wish to thank Thomas Foken, Head of the Department of Micrometeorology, University of Bayreuth, Germany, for helpful comments and discussions. Thanks to Professor K.T. Paw U from the University of California, Department of Land, Air and Water Resources, Davis, USA, for hosting K. Staudt during a 1-month stay at UC Davis and for supporting this work by numerous discussions. We are grateful to Matthias Mauder for assisting with TK2 calculations. We wish to acknowledge the help and technical support performed by the staff of the Bayreuth Center for Ecology and Environmental Research (BayCEER) of the University of Bayreuth. We greatly acknowledge the loan of the LAI2000 (LI-COR) instruments, and the forestry laser (Criterion 400, Laser Technology Inc. (LTI)) by Prof. Tenhunen, Plant Ecology, University of Bayreuth. The project is funded by the German Science Foundation (FO 226/16-1, ME2100/4-1, ZE 792/4-1) and by the Bavaria California Technology Center (BaCaTeC).

Appendix A. Appendix: Error estimation for sap flux measurements

Scaling sap flux measurements from tree to stand was done using a series of scaling parameters, and therefore involved propagation of uncertainties of sap flux readings and scaling parameters. In order to estimate the uncertainty in the calculated value of canopy transpiration (E_c), we used the Gaussian error propagation method (e.g. Taylor, 1997; Bevington and Robinson, 1992; Lo,

2005), described by

$$\sigma_{E_c}^2 = \sum_{i=1}^{n} \sigma_{x_i}^2 \left(\frac{\partial F}{\partial x_i}\right)^2 + \sum_{i=1}^{n}\sum_{j=1}^{n} \left(\left(\frac{\partial F}{\partial x_j}\right)\left(\frac{\partial F}{\partial x_i}\right)\sigma_{x_i}\sigma_{x_j} r\left(x_i, x_j\right)\right), \quad i \neq j \qquad (A.1)$$

where x_i, x_j are the variables or parameters used in the scaling function (F, equation (A.2), for the calculation of E_c, in W m^{-2}), σ_{xi} and σ_{xj} are their standard deviations, and $r(x_i, x_j)$ is the correlation coefficient between x_i and x_j. If the scaling parameters can be assumed to be uncorrelated, the variance of the scaled variable E_c, $\sigma_{E_c}^2$, is calculated from the variances of the parameters x as $\sigma_{E_c}^2 = \sum i(\sigma_x^2(\delta F/\delta x)^2)$, because in that case the covariance term ($\sigma_{xi} \cdot \sigma_{xj} \cdot r(x_i, x_j)$) is zero. Hence, the uncertainty of E_c, σ_{E_c}, the square root of $\sigma_{E_c}^2$, results from the associated uncertainties of the parameters. The scaling procedure employs repeated multiplication, and sums of a series of individual sap flux readings from outer and inner thermocouples (f_o, f_i, both m s^{-1}) and scaling parameters, for example outer and inner sapwood area ($A_{s,o}$, $A_{s,i}$, both m^2), representativeness of those readings for the entire stand (S_o, S_i, both unitless), or number of trees per m^2 (N):

$$F = \left(f_o \cdot A_{s,o} \cdot S_i + f_i \cdot A_{s,i} \cdot S_i\right) \cdot N \cdot L \cdot \rho \qquad (A.2)$$

where L latent heat of evaporation (2.45 MJ kg^{-1} at 20 °C), and ρ density of water (kg m^{-3}).

Each of the variables and parameters is associated with a given uncertainty (absolute, relative or derived from variances). Estimates for random and systematic uncertainties were identified for each measurement and determined from field calibration of the sensors (side-by-side measurements), and limits of detection; in more detail:

- For 1 week at the end of IOP-2 we installed seven sap flux sensors side-by-side in the stem of one tree. For use in the error propagation calculations we estimated from the standard deviation of the seven separate readings an uncertainty of 12.3% for the outer thermocouple readings ($\sigma_f = 0.085 \cdot f + 0.894 \times 10^{-6}$, f and σ_f in m s^{-1}), and 10.9% for the inner thermocouple reading ($\sigma_f = 0.069 \cdot f + 1.394 \times 10^{-6}$, f and σ_f in m s^{-1}). Because the measurements were performed side-by-side and post-processed before comparison, the accuracy here already includes the effects of radial variability, correction for wounding, and correction for deviation of thermal diffusivity from default, the latter being a function of thermal conductivity of fresh wood and of water; sapwood depth; fresh and dry weight, volume, and basic density of the wood core; density of water, and specific heat capacity of fresh wood, wood matrix and sap.
- The absolute errors of the cross-sectional area of the outer and inner rings of conducting sapwood area ($A_{s,o}$ and $A_{s,i}$) were estimated from errors of the circumference measurement (CH) and radial sapwood depth (D_{sw}) and were on average 10.3% of the respective sap wood area. The absolute error for the outer ring ($A_{s,o}$), with a radial depth of 0.002 m, varied between 0.00030 and 0.00245 m^2. The absolute error for the inner ring ($A_{s,i}$), with a variable radial depth (sapwood depth, D_{sw}, −0.002 m), varied between 0.00006 and 0.00750 m^2.
- Single tree sap flux was scaled to the stand scale using the representativeness of the two trees with sap flux sensor installations in tree profile for the entire stand, and the number of trees per m^2. As the two trees were comparatively large with respect to the CBH distribution of the entire stand (see Section 2.2.2), hourly correction factors were calculated from the ratio between stand estimates of E_c derived from sap flux measurements in seven trees (representing the CBH distribution of the entire stand) and stand estimates derived from the profile trees only. The correction factors were derived separately for inner and outer sap flux readings, and varied between 0.46 and 0.54 for the inner reading, and 0.56 and 0.69 for the outer reading, with relative errors of 11.4% and 14.0%, respectively.
- Single tree sap flux was scaled to the stand scale using the number of trees per m^2 (N) normally considered as an exact number. However, since the footprint of the eddy-covariance data is much larger than the subplot of the trees used for sap flux measurements, the number of trees per m^2 determined at the sap flux subplot might not represent the average value for the eddy-covariance footprint. In addition, its location varies with time. To address this mismatch at our relative heterogeneous site, we included an uncertainty estimate for the scaling factor N, determined from a variance analysis of the tree densities within the fenced area of the Waldstein–Weidenbrunnen site. Variances of N were calculated for subplots of different size (100–5000 m^2, limited by the extent of the fenced area, where all tree positions were measured). The relative error estimated from the variance for N was highest (43%) at subplot size 100 m^2, and declined with increasing subplot size to level off to 20% at subplot sizes larger than 2500 m^2. For the error propagation analysis we used the value of 40%, even though for an extension of the subplot size beyond the fenced area an increase of the variances in tree density is expected due to clearings and stands of other age-classes nearby.

Solving the partial derivatives of equation ((A.2), F), and substituting those and the above error estimates in equation (A.1), the final error of an individual estimate of E_c is calculated.

Covariance terms were not considered for correlation between average f and A_s ($f = -2.66 \times 10^{-5} \cdot A_s + 1.15 \times 10^{-5}$, $r = 0.071$, f in m s^{-1}), nor for correlation between S and N. However, significant correlations were found between $f \cdot A_s$ and N, ($f \cdot A_s = -2.30 \times 10^{-10} \cdot N + 0.56 \times 10^{-10}$, $r = -0.89$, $f \cdot A_s$ in m^3 s^{-1}, our data and data from Alsheimer, 1997), and inner and outer ring estimates (for all levels strong linear relations were found with r ranging between 0.940 and 0.997). Appropriate covariance terms were considered in the latter cases.

When individual estimates are aggregated over a time period, propagation of measurement uncertainty during aggregation has to be performed. The sap flux estimates were aggregated from 10-min time resolution to 30-min resolution to match the eddy-covariance data. This reduced the final error estimate by a factor of approximately $1/\sqrt{3}$, because for an aggregation of n measurements with equal relative errors, random errors diminish with increasing n according to $1/\sqrt{n}$ (Taylor, 1997).

References

Akima, H., 1978. A method of bivariate interpolation and smooth surface fitting for irregularly distributed data points. ACM Trans. Math. Softw. 4, 148–159.

Alsheimer, M., 1997. Charakterisierung räumlicher und zeitlicher Heterogenität der Transpiration unterschiedlicher montaner Fichtenbestände (*Picea abies* (L.) KARST.) durch Xylemflußmessungen, vol. 49. Bayreuther Forum Ökologie, 143 pp.

Aubinet, M, Grelle, A., Ibrom, A., Rannik, Ü., Moncrieff, J., Foken, T., Kowalski, A.S., Martin, P.H., Berbigier, P., Bernhofer, C., Clement, R., Elbers, J., Granier, A., Grünwald, T., Morgenstern, K., Pilegaard, K., Rebmann, C., Snijders, W., Valentini, R., Vesala, T., 2000. Estimates of the annual net carbon and water exchange of forests: the EUROFLUX methodology. Adv. Ecol. Res. 30, 113–175.

Baldocchi, D., 1997. Flux footprints within and over forest canopies. Boundary-Layer Meteorol. 85, 273–292.

Baldocchi, D.D., 2003. Assessing the eddy covariance technique for evaluating carbon dioxide exchange rates of ecosystems: past, present and future. Global Change Biol. 9, 479–492.

Baldocchi, D.D., Meyers, T.P., 1991. Trace gas exchange above the floor of a deciduous Forest 1. Evaporation and CO_2 efflux. J. Geophys. Res. – Atmospheres 96, 7271–7285.

Baldocchi, D.D., Vogel, C.A., 1996. Energy and CO_2 flux densities above and below a temperate broad-leaved forest and a boreal pine forest. Tree Physiol. 16, 5–16.
Baldocchi, D.D., Law, B.E., Anthoni, P.M., 2000. On measuring and modeling energy fluxes above the floor of a homogeneous and heterogeneous conifer forest. Agric. For. Meteorol. 102, 187–206.
Barbour, M.M., Hunt, J.E., Walcroft, A.S., Rogers, G.N., McSeveny, T.M., Whitehead, D., 2005. Components of ecosystem evaporation in a temperate coniferous rainforest, with canopy transpiration scaled using sapwood density. New Phytol. 165, 549–558.
Bevington, P.R., Robinson, D.K., 1992. Data Reduction and Error Analysis for the Physical Sciences. McGraw-Hill, New York, 328 pp.
Burgess, S.S.O., Adams, M., Turner, N.C., Beverly, C.R., Ong, C.K., Khan, A.A., Bleby, T.M., 2001. An improved heat pulse method to measure low and reverse rates of sap flow in woody plants. Tree Physiol. 21, 589–598.
Burgess, S.S.O., Adams, M.A., Bleby, T.M., 2000. Measurement of sap flow in roots of woody plants: a commentary. Tree Physiol. 20, 909–913.
Burgess, S.S.O., Adams, M.A., Turner, N.C., Ong, C.K., 1998. The redistribution of soil water by tree root systems. Oecologia 115, 306–311.
Campbell, G.S., 1985. Soil Physics with BASIC. Elsevier, Amsterdam, 150 pp.
Caylor, K.K., Dragoni, D., 2009. Decoupling structural and environmental determinants of sap velocity: Part I methodological development. Agric. For. Meteorol. 149, 559–569.
Cermak, J., Nadezhdina, N., 1998. Sapwood as the scaling parameter-defining according to xylem water content or radial pattern of sap flow? Ann. For. Sci. 55, 509–521.
Chang, M., 2006. Forest Hydrology. An Introduction to Water and Forests. Taylor & Francis, Boca Raton, 474 pp.
Collatz, G.J., Ball, J.T., Grivet, C., Berry, J.A., 1991. Physiological and environmental regulation of stomatal conductance, photosynthesis and transpiration: a model that includes a laminar boundary layer. Agric. For. Meteorol. 54, 107–136.
Czikowsky, M.J., Fitzjarrald, D.R., 2009. Detecting rainfall interception in an Amazonian rain forest with eddy flux measurements. J. Hydrol. 377, 92–105.
Davi, H., Dufrêne, E., Granier, A., Le Dantec, V., Barbaroux, C., François, C., Bréda, N., 2005. Modelling carbon and water cycles in a beech forest: Part II. Validation of the main processes from organ to stand scale. Ecol. Model. 185, 387–405.
Dragoni, D., Caylor, K.K., Schmid, H.P., 2009. Decoupling structural and environmental determinants of sap velocity: Part II. Observational application. Agric. For. Meteorol. 149, 570–581.
Falge, E., 1997. Die Modellierung der Kronendachtranspiration von Fichtenbeständen (*Picea abies* (L.) KARST.), vol. 48. Bayreuther Forum Ökologie, 215 pp.
Falge, E., Meixner, F.X., 2008. Validation of a 3D gas exchange model for a *Picea abies* canopy in the Fichtelgebirge, Germany. Geophys. Res. Abstr. 10, EGU2008-A-07272 SRef-ID: 1607-7962/gra/EGU2008-A-07272.
Falge, E., Reth, S., Brüggemann, N., Butterbach-Bahl, K., Goldberg, V., Oltchev, A., Schaaf, S., Spindler, G., Stiller, B., Queck, R., Köstner, B., Bernhofer, C., 2005. Comparison of surface energy exchange models with eddy flux data in forest and grassland ecosystems of Germany. Ecol. Model. 188, 174–216.
Falge, E., Tenhunen, J.D., Ryel, R., Alsheimer, M., Köstner, B., 2000. Modelling age- and density-related gas exchange of *Picea abies* canopies in the Fichtelgebirge Germany. Ann. For. Sci. 57, 229–243.
Farquhar, G.D., von Caemmerer, S., 1982. Modelling of photosynthetic response to environmental conditions. In: Lange, O.L., Nobel, P.S., Osmond, C.B., Ziegler, H. (Eds.), Physiological Plant Ecology II, Water Relations and Carbon Assimilation. Springer, Berlin, pp. 549–588.
FLUXNET, 2010. http://daac.ornl.gov/FLUXNET/, accessed: 23.03.2010.
Foken, T., 2003. Lufthygienisch-bioklimatische Kennzeichnung des oberen Egertales (Fichtelgebirge bis Karlovy Vary), vol. 100. Bayreuther Forum Ökologie, 70 pp.
Foken, T., 2008. The energy balance closure problem: An overview. Ecol. Appl. 18, 1351–1367.
Foken, T., Göckede, M., Mauder, M., Mahrt, L., Amiro, B.D., Munger, J.W., 2004. Post-field data quality control. In: Lee, X., Massman, W., Law, B. (Eds.), Handbook of Micrometeorology: A Guide for Surface Flux Measurements. Kluwer, Dordrecht, pp. 81–108.
Foken, T., Meixner, F.X., Falge, E., Zetzsch, C., Serafimovich, A., Balzer, N., Bargsten, A., Behrendt, T., Lehmann-Pape, L., Hens, K., Jocher, G., Kesselmeier, J., Lüers, J., Mayer, J.-C., Moravek, A., Plake, D., Riederer, M., Rütz, F., Schier, S., Siebicke, L., Sörgel, M., Staudt, K., Trebs, I., Tsokankunku, A., Wolff, V., Zhu, Z. Atmospheric transport and chemistry in forest ecosystems – overview of the EGER-Project. Agric. For. Meteorol., in preparation.
Ford, C.R., McGuire, M.A., Mitchell, R.J., Teskey, R.O., 2004. Assessing variation in the radial profile of sap flux density in Pinus species and its effect on daily water use. Tree Physiol. 24, 241–249.
Frankenberger, E., 1951. Untersuchungen über den Vertikalaustausch in den unteren Dekametern der Atmosphäre. Ann. Meteorol. 4, 358–374.
Frühauf, C., Zimmermann, L., Bernhofer, C., 1999. Comparison of forest evapotranspiration from ECEB-measurements over a spruce stand with the water budget of a catchment. Phys. Chem. Earth B 24, 805–808.
Gerstberger, P., Foken, T., Kalbitz, K., 2004. The Lehstenbach and Steinkreuz catchments in NE Bavaria Germany. In: Matzner, E. (Ed.), Biogeochemistry of Forested Catchments in a Changing Environment: A German Case Study. Ecological Studies 172. Springer, Berlin, Heidelberg, pp. 15–44.
Göckede, M., Foken, T., Aubinet, M., Aurela, M., Banza, J., Bernhofer, C., Bonnefond, J.M., Brunet, Y., Carrara, A., Clement, R., Dellwik, E., Elbers, J., Eugster, W., Fuhrer, J., Granier, A., Grünwald, T., Heinesch, B., Janssens, I.A., Knohl, A., Koeble, R., Laurila, T., Longdoz, B., Manca, G., Marek, M., Markkanen, T., Mateus, J., Matteucci, G., Mauder, M., Migliavacca, M., Minerbi, S., Moncrieff, J., Montagnani, L., Moors, E., Ourcival, J.M., Papale, D., Pereira, J., Pilegaard, K., Pita, G., Rambal, S., Rebmann, C., Rodrigues, A., Rotenberg, E., Sanz, M.J., Sedlak, P., Seufert, G., Siebicke, L., Soussana, J.F., Valentini, R., Vesala, T., Verbeeck, H., Yakir, D., 2008. Quality control of CarboEurope flux data – Part 1: coupling footprint analyses with flux data quality assessment to evaluate sites in forest ecosystems. Biogeosciences 5, 433–450.
Granier, A., Biron, P., Bréda, N., Pontailler, J.Y., Saugier, B., 1996. Transpiration of trees and forest stands: short and long-term monitoring using sapflow methods. Global Change Biol. 2, 265–274.
Granier, A., Biron, P., Lemoine, D., 2000. Water balance, transpiration and canopy conductance in two beech stands. Agric. For. Meteorol. 100, 291–308.
Granier, A., Loustau, D., 1994. Measuring and modelling the transpiration of a maritime pine canopy from sap-flow data. Agric. For. Meteorol. 71, 61–81.
Green, S.R., Clothier, B.E., 1988. Water use of Kiwifruit Vines and Apple trees by the heat-pulse technique. J. Exp. Bot. 39, 115–123.
Green, S., Clothier, B., Jardine, B., 2003. Theory and practical application of heat pulse to measure sap flow. Agron. J. 95, 1371–1379.
Hatton, T.J., Moore, S.J., Reece, P.H., 1995. Estimating stand transpiration in a Eucalyptus populnea woodland with the heat pulse method: measurement errors and sampling strategies. Tree Physiol. 15, 219–227.
Hatton, T.J., Vertessy, R.A., 1990. Transpiration of plantation *Pinus radiata* estimated by the heat pulse method and the bowen ratio. Hydrol. Processes 4, 289–298.
Hatton, T.J., Wu, H.-I., 1995. Scaling theory to extrapolate individual tree water use to stand water use. Hydrol. Processes 9, 527–540.
Heindl, B., Ostendorf, B., Köstner, B., 1995. Lage und forstliche Charakterisierung des Einzugsgebietes Lehstenbach. In: Manderscheid, B., Göttlein, A. (Eds.), Wassereinzugsgebiet 'Lehstenbach' – das BITÖK-Untersuchungsgebiet am Waldstein (Fichtelgebirge NO-Bayern), vol. 18. Bayreuther Forum Ökologie, pp. 7–14.
Hendl, M., 1991. Globale Klimaklassifikation. In: Hupfer, P. (Ed.), Das Klimasystem der Erde. Diagnose und Modellierung, Schwankungen und Wirkungen. Akad.-Verl, Berlin, pp. 218–266.
Jarosz, N., Brunet, Y., Lamaud, E., Irvine, M., Bonnefond, J.M., Loustau, D., 2008. Carbon dioxide and energy flux partitioning between the understorey and the overstorey of a maritime pine forest during a year with reduced soil water availability. Agric. For. Meteorol. 148, 1508–1523.
Juang, J.Y., Katul, G., Siqueira, M.B., Stoy, P.C., McCarthy, H.R., 2008. Investigating a hierarchy of Eulerian closure models for scalar transfer inside forested canopies. Boundary-Layer Meteorol. 128, 1–32.
Kellomäki, S., Wang, K.-Y., 1999. Short-term environmental controls of heat and water vapour fluxes above a boreal coniferous forest: model computations compared with measurements by eddy correlation. Ecol. Model. 124, 145–173.
Klemm, O., Wrzesinsky, T., 2007. Fog deposition fluxes of water and ions to a mountainous site in Central Europe. Tellus B 59, 705–714.
Köstner, B.M.M., Schulze, E.D., Kelliher, F.M., Hollinger, D.Y., Byers, J.N., Hunt, J.E., McSeveny, T.M., Meserth, R., Weir, P.L., 1992. Transpiration and canopy conductance in a pristine broad-leaved forest of Nothofagus: an analysis of xylem sap flow and eddy correlation measurements. Oecologia 91, 350–359.
Köstner, B., 1999. Die Transpiration von Wäldern – Quantifizierung als Xylemsaftfluss und Faktorenabhängigkeit von Teilflüssen. Habilitation thesis, University of Bayreuth, 283 pp.
Köstner, B., Biron, P., Siegwolf, R., Granier, A., 1996. Estimates of water vapor flux and canopy conductance of Scots pine at the tree level utilizing different xylem sap flow methods. Theor. Appl. Climatol. 53, 105–113.
Köstner, B., Falge, E.M., Alsheimer, M., Geyer, R., Tenhunen, J.D., 1998. Estimating tree canopy water use via xylem sapflow in an old Norway spruce forest and a comparison with simulation-based canopy transpiration estimates. Ann. Sci. For. 55, 125–139.
Kumagai, T., Aoki, S., Nagasawa, H., Mabuchi, T., Kubota, K., Inoue, S., Utsumi, Y., Otsuki, K., 2005. Effects of tree-to-tree and radial variations on sap flow estimates of transpiration in Japanese cedar. Agric. For. Meteorol. 135, 110–116.
Kumagai, T., Aoki, S., Otsuki, K., Utsumi, Y., 2009. Impact of stem water storage on diurnal estimates of whole-tree transpiration and canopy conductance from sap flow measurements in Japanese cedar and Japanese cypress trees. Hydrol. Processes 23, 2335–2344.
Kurpius, M.R., Panek, J.A., Nikolov, N.T., Mckay, M., Goldstein, A.H., 2003. Partitioning of water flux in a Sierra Nevada ponderosa pine plantation. Agric. For. Meteorol. 117, 173–192.
Lassoie, J.P., Scott, D.R., Fritschen, L.J., 1977. Transpiration studies in Douglas-fir using heat pulse technique. For. Sci. 23, 377–390.
Leuning, R., 1990. Modelling stomatal behaviour and photosynthesis of *Eucalyptus grandis*. Aust. J. Plant Physiol. 17, 159–175.
Lo, E., 2005. Gaussian error propagation applied to ecological data: post-ice-storm-downed woody biomass. Ecol. Monogr. 75, 451–466.
Lundblad, M., Lindroth, A., 2002. Stand transpiration and sapflow density in relation to weather, soil moisture and stand characteristics. Basic Appl. Ecol. 3, 229–243.
Marras, S., 2008. Evaluation of the "Advanced Canopy-Atmosphere-Soil Algorithm" (ACASA) model performance using micrometeorological techniques. PhD thesis, Università degli Studi di Sassari, Sassari, Italy, 263 pp.
Mauder, M., Foken, T., 2004. Documentation and instruction 1 manual of the eddy covariance software package TK2. Arbeitsergebnisse, Universität Bayreuth, Abt. Mikrometeorologie, ISSN 1614-8916, 26, 45 pp.
Mauder, M., Liebethal, C., Göckede, M., Leps, J.-P., Beyrich, F., Foken, T., 2006. Processing and quality control of flux data during LITFASS-2003. Boundary-Layer Meteorol. 121, 67–88.
Mauder, M., Oncley, S.P., Vogt, R., Weidinger, T., Ribeiro, L., Bernhofer, C., Foken, T., Kohsiek, W., Bruin, H.A.R., de Liu, H., 2007. The energy balance experiment

EBEX-2000 Part II: Intercomparison of eddy-covariance sensors and post-field data processing methods. Boundary-Layer Meteorol. 123, 29–54.
McNaughton, K.G., Jarvis, P.G., 1983. Predicting effects of vegetation changes on transpiration and evaporation. In: Kozlowski, T.T. (Ed.), Water Deficits and Plant Growth. Academic Press, Inc., New York, pp. 1–47.
Meyers, T.P., 1985. A simulation of the canopy microenvironment using higher order closure principles. PhD thesis, Purdue University, 153 pp.
Meyers, T.P., Paw, U.K.T., 1986. Testing of a higher-order closure model for airflow within and above plant canopies. Boundary-Layer Meteorol. 37, 297–311.
Meyers, T.P., Paw, U.K.T., 1987. Modelling the plant canopy micrometeorology with higher-order closure techniques. Agric. For. Meteorol. 41, 143–163.
Moldrup, P., Rolston, D.E., Hansen, J.A.A., 1989. Rapid and numerically stable simulation of one-dimensional, transient water-flow in unsaturated, layered soils. Soil Sci. 148, 219–226.
Moldrup, P., Rolston, D.E., Hansen, J.A.A., Yamaguchi, T., 1992. A simple mechanistic model for soil resistance to plant water uptake. Soil Sci. 153, 87–93.
Nadezhdina, N., Cermak, J., Ceulemans, R., 2002. Radial patterns of sap flow in woody stems of dominant and understory species: scaling errors associated with positioning of sensors. Tree Physiol. 22, 907–918.
Oishi, A.C., Oren, R., Stoy, P.C., 2008. Estimating components of forest evapotranspiration: a footprint approach for scaling sap flux measurements. Agric. For. Meteorol. 148, 1719–1732.
Oren, R., Phillips, N., Katul, G., Ewers, B.E., Pataki, D.E., 1998. Scaling xylem sap flux and soil water balance and calculating variance: a method for partitioning water flux in forests. Ann. Sci. For. 55, 191–216.
Park, H., Hattori, S., 2004. Modeling scalar and heat sources, sinks, and fluxes within a forest canopy during and after rainfall events. J. Geophys. Res. – Atmospheres 109, D14301.
Paw, U.K.T., Gao, W., 1988. Applications of solutions to non-linear energy budget equations. Agric. For. Meteorol. 43, 121–145.
Phillips, N., Nagchaudhuri, A., Oren, R., Katul, G., 1997. Time constant for water transport in loblolly pine trees estimated from time series of evaporative demand and stem sapflow. Trees – Struct. Funct. 11, 412–419.
Phillips, N., Oren, R., Zimmermann, R., 1996. Radial patterns of xylem sap flow in non-, diffuse- and ring-porous tree species. Plant Cell Environ. 19, 983–990.
Phillips, N., Bond, B.J., McDowell, N.G., Ryan, M.G., 2002. Canopy and hydraulic conductance in young, mature and old Douglas-fir trees. Tree Physiol. 22, 205–211.
Poyatos, R., Cermak, J., Llorens, P., 2007. Variation in the radial patterns of sap flux density in pubescent oak (*Quercus pubescens*) and its implications for tree and stand transpiration measurements. Tree Physiol. 27, 537–548.
Pyles, R.D., 2000. The development and testing of the UCD advanced canopy-atmosphere soil algorithm (ACASA) for use in climate prediction and field studies. PhD thesis, UC Davis, 194 pp.
Pyles, R.D., Weare, B.C., Paw, U.K.T., 2000. The UCD advanced canopy-atmosphere-soil algorithm: comparisons with observations from different climate and vegetation regimes. Q. J. R. Meteorol. Soc. 126, 2951–2980.
R Development Core Team, 2008. R: A Language and Environment for Statistical Computing. R Foundation for Statistical Computing, Vienna, Austria, http://www.R-project.org.
Rawls, W.J., Brakensiek, D.L., 1989. Estimation of soil water retention and hydraulic properties. Unsaturated flow in hydrologic modeling. In: Morel-Seytoux, H.J. (Ed.), Theory and Practice; Proceedings of the NATO Advanced Research Workshop on Unsaturated Flow in Hydrologic Modeling Arles France 13–17 June 1988. Kluwer, Dordrecht, pp. 275–300.
Rebmann, C., 2004. Kohlendioxid-Wasserdampf- und Energieaustausch eines Fichtenwaldes in Mittelgebirgslage in Nordostbayern, vol. 106. Bayreuther Forum Ökologie, p. 140.
Richard, L.A., 1931. Capillary conductivity of liquids in porous mediums. Physics 1, 318–333.
Rochette, P., Hutchinson, G.L., 2005. Measurement of soil respiration in situ: chamber techniques. In: Hatfield, J.L., Baker, J.M., Viney, M.K. (Eds.), Micrometeorology in Agricultural Systems. American Soc. of Agronomy, Madison, Wis, pp. 247–286.
Roupsard, O., Bonnefond, J.M., Irvine, M., Berbigier, P., Nouvellon, Y., Dauzat, J., Taga, S., Hamel, O., Jourdan, C., Saint-Andre, L., Mialet-Serra, I., Labouisse, J.P., Epron, D., Joffre, R., Braconnier, S., Rouziere, A., Navarro, M., Bouillet, J.P., 2006. Partitioning energy and evapo-transpiration above and below a tropical palm canopy. Agric. For. Meteorol. 139, 252–268.
Saugier, B., Granier, A., Pontailler, J.Y., Dufrene, E., Baldocchi, D.D., 1997. Transpiration of a boreal pine forest measured by branch bag, sap flow and micrometeorological methods. Tree Physiol. 17, 511–519.
Schulze, E.D., Čermák, J., Matyssek, M., Penka, M., Zimmermann, R., Vasícek, F., Gries, W., Kučera, J., 1985. Canopy transpiration and water fluxes in the xylem of the trunk of Larix and Picea Trees – a comparison of xylem flow, porometer and cuvette measurements. Oecologia 66, 475–483.
Serafimovich, A., Siebicke, L., Staudt, K., Lüers, J., Biermann, T.S.S., Mayer, J.-C., Foken, T., 2008. ExchanGE Processes in Mountainous Regions (EGER): Documentation of the Intensive Observation Period (IOP1) September 6th to October 7th 2007. Arbeitsergebnisse, Universität Bayreuth, Abt. Mikrometeorologie, ISSN1614-8916, 36, 147 pp.
Serafimovich, A., Siebicke, L., Staudt, K., Lüers, J., Hunner, M., Gerken, T., Schier, S., Biermann, T., Rütz, F., Buttlar, J. von, Riederer, M., Falge, E., Mayer, J.-C., Foken, T., 2008. ExchanGE Processes in Mountainous Regions (EGER): Documentation of the Intensive Observation Period (IOP2) June 1st to July 15th 2008. Arbeitsergebnisse, Universität Bayreuth, Abt. Mikrometeorologie, ISSN1614-8916, 37, 180 pp.
Siebicke, L., 2008. Footprint synthesis for 1 the FLUXNET site Waldstein/Weidenbrunnen (DE-Bay) during the EGER experiment. Arbeitsergebnisse, Universität Bayreuth, Abt. Mikrometeorologie, ISSN1614-8916, 38, 45 pp.
Siebicke, L., Serafimovich, A., Foken, T., 2010. Linking CO_2-advection estimates to vegetation structure at a forest site. Agric. For. Meteorol., in preparation.
Smirnova, T.G., Brown, J.M., Benjamin, S.G., 1997. Performance of different soil model configurations in simulating ground surface temperature and surface fluxes. Mon. Weather Rev. 125, 1870–1884.
Smirnova, T.G., Brown, J.M., Benjamin, S.G., Kim, D., 2000. Parameterization of cold-season processes in the MAPS land-surface scheme. J. Geophys. Res. – Atmospheres 105, 4077–4086.
Staudt, K., Falge, E., Pyles, R.D., Foken, T., 2010. Sensitivity and predictive uncertainty of the ACASA model at a spruce forest site. Biogeosci. Discuss. 7, 4223–4271.
Su, H.B., Paw, U.K.T., Shaw, R.H., 1996. Development of a coupled leaf and canopy model for the simulation of plant-atmosphere interactions. J. Appl. Meteorol. 35, 733–748.
Tang, J., Bolstad, P.V., Ewers, B.E., Desai, A.R., Davis, K.J., Carey, E.V., 2006. Sap flux–upscaled canopy transpiration, stomatal conductance, and water use efficiency in an old growth forest in the Great Lakes region of the United States. J. Geophys. Res. – Biogeosci. 111, G02009.
Taylor, J.R., 1997. An Introduction to Error Analysis. The Study of Uncertainties in Physical Measurements. University Science Books, Sausalito, California, 327 pp.
Thomas, C., Foken, T., 2005. Detection of long-term coherent exchange over spruce forest using wavelet analysis. Theor. Appl. Climatol. 80, 91–104.
Thomas, C., Foken, T., 2007a. Flux contribution of coherent structures and its implications for the exchange of energy and matter in a tall spruce canopy. Boundary-Layer Meteorol. 123, 317–337.
Thomas, C., Foken, T., 2007b. Organised motion in a tall spruce canopy: temporal scales, structure spacing and terrain effects. Boundary-Layer Meteorol. 122, 123–147.
van Genuchten, M.T., 1980. A Closed-form equation for predicting the hydraulic conductivity of unsaturated soils. Soil Sci. Soc. Am. J. 44, 892–898.
Vertessy, R.A., Benyon, R.G., O'Sullivan, S.K., Gribben, P.R., 1995. Relationships between stem diameter, sapwood area, leaf area and transpiration in a young mountain ash forest. Tree Physiol. 15, 559–567.
Wang, K.-Y., Kellomäki, S., Zha, T., Peltola, H., 2004. Seasonal variation in energy and water fluxes in a pine forest: an analysis based on eddy covariance and an integrated model. Ecol. Model. 179, 259–279.
Willmott, C., 1982. Some comments on the evaluation of model performance. Bull. Am. Meteorol. Soc. 63, 1309–1313.
Wilson, K.B., Hanson, P.J., Baldocchi, D.D., 2000. Factors controlling evaporation and energy partitioning beneath a deciduous forest over an annual cycle. Agric. For. Meteorol. 102, 83–103.
Wilson, K.B., Hanson, P.J., Mulholland, P.J., Baldocchi, D.D., Wullschleger, S.D., 2001. A comparison of methods for determining forest evapotranspiration and its components: sap-flow, soil water budget, eddy covariance and catchment water balance. Agric. For. Meteorol. 106, 153–168.
Wilson, K.B., Meyers, T.P., 2001. The spatial variability of energy and carbon dioxide fluxes at the floor of a deciduous forest. Boundary-Layer Meteorol. 98, 443–473.
Wullschleger, S.D., King, A.W., 2000. Radial variation in sap velocity as a function of stem diameter and sapwood thickness in yellow-poplar trees. Tree Physiol. 20, 511–518.
Wullschleger, S.D., Meinzer, F.C., Vertessy, R.A., 1998. A review of whole-plant water use studies in tree. Tree Physiol. 18, 499–512.
Wullschleger, S.D., Norby, R.J., 2001. Sap velocity and canopy transpiration in a sweetgum stand exposed to free-air CO_2 enrichment (FACE). New Phytol. 150, 489–498.
Yaseef, N.R., Yakir, D., Rotenberg, E., Schiller, G., Cohen, S., 2009. Ecohydrology of a semi-arid forest: partitioning among water balance components and its implications for predicted precipitation changes. Ecohydrology, doi:10.1002/eco.65.
Zimmermann, L., Frühauf, C., Bernhofer, C., 1999. The role of interception in the water budget of spruce stands in the Eastern Ore Mountains/Germany. Phys. Chem. Earth B 24, 809–812.

Please cite this article in press as: Staudt, K., et al., Vertical structure of evapotranspiration at a forest site (a case study). Agric. Forest Meteorol. (2010), doi:10.1016/j.agrformet.2010.10.009